LASER ATMOSPHERIC PROPAGATION KINETICS

C. A. Brau, et al

Avco Everett Research Laboratory, Incorporated

Prepared for:

Office of Naval Research
Advanced Research Projects Agency

June 1974

UNCLASSIFIED

SECURITY CLASSIFICATION OF THIS PAGE *(When Data Entered)*

AD- 782416

REPORT DOCUMENTATION PAGE		READ INSTRUCTIONS BEFORE COMPLETING FORM
1. REPORT NUMBER	2. GOVT ACCESSION NO.	3. RECIPIENT'S CATALOG NUMBER
4. TITLE *(and Subtitle)* LASER ATMOSPHERIC PROPAGATION KINETICS		5. TYPE OF REPORT & PERIOD COVERED Final Technical Report-Phase I May 1, 1973 - Dec. 31, 1973 6. PERFORMING ORG. REPORT NUMBER
7. AUTHOR(s) C. A. Brau, E. R. Bressel, S. L. Glickler		8. CONTRACT OR GRANT NUMBER(s) N00014-73-C-0311
9. PERFORMING ORGANIZATION NAME AND ADDRESS Avco Everett Research Laboratory, Inc. 2385 Revere Beach Parkway Everett, Massachusetts 02149		10. PROGRAM ELEMENT, PROJECT, TASK AREA & WORK UNIT NUMBERS
11. CONTROLLING OFFICE NAME AND ADDRESS		12. REPORT DATE June 1974 13. NUMBER OF PAGES 63
14. MONITORING AGENCY NAME & ADDRESS *(if different from Controlling Office)* ARPA, DOD, and monitored by Office of Naval Research, Department of the Navy, Arlington, Virginia 22217		15. SECURITY CLASS. *(of this report)* Unclassified 15a. DECLASSIFICATION/DOWNGRADING SCHEDULE

16. DISTRIBUTION STATEMENT *(of this Report)*

Approved for Public Release; Distribution Unlimited

17. DISTRIBUTION STATEMENT *(of the abstract entered in Block 20, if different from Report)*

18. SUPPLEMENTARY NOTES

19. KEY WORDS *(Continue on reverse side if necessary and identify by block number)*

Laser Propagation
Laser Absorption
Vibrational Relaxation
Rotational Relaxation
Atmospheric Absorption

20. ABSTRACT *(Continue on reverse side if necessary and identify by block number)*

A model has been developed to describe the kinetics of absorption of DF and CO radiation by the atmosphere. The model has been exercised for pulsed lasers to determine the atmospheric temperature change resulting from this absorption. Calculations were performed both at sea level and at an altitude of 12 km for two limiting concentrations of water and for laser energies varying over several orders of magnitude. The results for DF indicate that N_2O will bleach at intensities of 10^6 to 10^8 W/cm^2, depending on the pressure and humidity. Absorption of CO laser radiation by H_2O and

DD FORM 1 JAN 73 1473 EDITION OF 1 NOV 65 IS OBSOLETE

UNCLASSIFIED

SECURITY CLASSIFICATION OF THIS PAGE *(When Data Entered)*

LASER ATMOSPHERIC PROPAGATION KINETICS

FINAL TECHNICAL REPORT - PHASE I
(1 May 1973 - 31 December 1973)

by

C. A. Brau, E. R. Bressel and S. L. Glickler

AVCO EVERETT RESEARCH LABORATORY, INC.
a Subsidiary of Avco Corporation
Everett, Massachusetts

Contract No. N00014-73-C-0311

June 1974

supported by

ADVANCED RESEARCH PROJECTS AGENCY
DEPARTMENT OF DEFENSE

and

monitored by

OFFICE OF NAVAL RESEARCH
DEPARTMENT OF THE NAVY
Arlington, Virginia 22217

ib

FOREWORD

ARPA Order No. 1806

Program Code No. 3E90

Name of Contractor: Avco Everett Research Laboratory, Inc.

Effective Date of Contract: May 1, 1973

Contract Expiration Date: December 31, 1973

Amount of Contract: $63,028

Contract No: N00014-73-C-0311

Principal Investigator and Phone No: C. A. Brau - (617)389-3000, Ext. 532

Scientific Officer: Director, Physics Program, Physical Sciences Division
Office of Naval Research Department of the Navy,
Arlington, Virginia 22217

Short Title of Work: Propagation Kinetics

The AERL personnel who authored this report are Dr. Charles A. Brau, Dr. Ellen R. Bressel and Mr. Sheldon L. Glickler.

The authors gratefully acknowledge the contributions of Drs. Lee A. Young, Bennet Kivel and C. Bradley Moore to this program.

SUMMARY

PURPOSE

The purpose of this program was to develop an analytical model describing the atmospheric absorption of laser energy and the subsequent kinetic processes of energy exchange. The final result of this effort is the quantitative determination of the atmospheric temperature change resulting from this absorption.

The major effort has been concentrated on the DF laser system. Eight representative strong laser transitions were selected. The atmospheric absorbers, energy levels and absorption cross sections have been specified. The analytical kinetic model has been developed and rate constants have been selected for use in the calculation. With a simple square wave pulse shape, the model has been used to give an assessment of the kinetic effects of the absorbers in heating the atmosphere both at sea level and at an altitude of 12 kilometers. Two limiting concentrations of water have been used and the laser energy has been varied over several orders of magnitude. The results are summarized below and detailed in subsequent sections. The sea level atmospheric temperature change resulting from absorption of CO laser energy by atmospheric water is also given.

CONCLUSIONS

A model has been developed to describe the kinetics of absorption of DF and CO laser radiation by the atmosphere.

DF laser radiation is absorbed by N_2 (collision induced continuum band), CO_2 (ν_3), N_2O ($2\nu_1$ and $\nu_1 + 2\nu_2$), CH_4 ($2\nu_4$ and $\nu_2 + \nu_4$), HDO (ν_1) and H_2O (ν_2 and $2\nu_2$) and the H_2O continuum. Most of the absorption bands from the ground vibrational level are well documented in the literature, but considerable discrepancies exist concerning absorption by H_2O and HDO. No information is available regarding absorption from the upper vibrational levels, and these have been ignored. Under conditions when the absorbing transition is bleached, this may become a severe limitation for the model. CO laser radiation is absorbed by CO_2 and H_2O. Of these two, H_2O (ν_2) is overwhelmingly the most important band, and this band is well documented in the literature.

The kinetics model describes the vibrational relaxation of these absorbing species in considerable detail. Rotational relaxation is shown to be unimportant for intensities below 10^{10} W/cm^2. Considerable information exists regarding the relaxation of N_2, CO_2 (ν_3), CH_4 (ν_2 and ν_4) and H_2O (ν_2). However, very little useful information exists regarding

the relaxation of N_2O (ν_1 and ν_2) and HDO (ν_1). Since the relaxation of HDO is presumed (by analogy to H_2O) to be very fast, these rates are not too critical. However, N_2O is an important absorber and the effects of vibrational relaxation in N_2O are significant. Thus, the order-of-magnitude uncertainties which exist in some of the important N_2O relaxation processes represent a serious limitation in the model.

Preliminary results have been obtained for the absorption of CO and DF radiation under a variety of conditions. The results indicate that N_2O will bleach at intensities of 10^6 to 10^8 W/cm^2, depending on the pressure and humidity. Under conditions of very low humidity, absorption by CH_4 will cause cooling of the atmosphere for short times. Absorption of CO laser radiation by H_2O (ν_2) and subsequent heating of the atmosphere is much stronger than any of the processes affecting DF. Under conditions of low humidity, however, V-V transfer from H_2O (ν_2) to O_2 will slow the rate of heating of the atmosphere.

TABLE OF CONTENTS

LIST OF ILLUSTRATIONS

I. SPECTROSCOPY

A. SELECTION OF DF LASER TRANSITIONS

In a DF chemical laser the DF molecules are formed by chemical reaction in high vibrational and rotational states. As they lase and relax by collisional processes they cascade down to lower, thermally populated levels. Thus, in pulsed DF lasers the various transitions do not all lase simultaneously. Rather, the higher vibrational levels tend to lase first with lower levels appearing later in the pulse. Even in continuous wave (CW) lasers the relative strength of the various lines is a complex function of the chemical and relaxation processes occuring in the laser. The various DF lines are absorbed by different species with widely varying absorption cross sections. Therefore, it may be found desirable to suppress certain transitions, even though they may be strong laser lines, if they are strongly absorbed and adversely affect the propagation of other lines. However, this may be difficult to accomplish in DF lasers due to their intrinsic high gain and the complex nature of the processes controlling the relative strength of the various lines.

The eight DF laser transitions shown in Table I were chosen from the experimental work on pulsed DF lasers of Deutsch[1] and Basov, et al.[2] Reference 1, which contains the most accurate experimental measurements of line position (± 0.08 cm^{-1}), was used to determine the transition frequency, and the relative energy data of Ref. 2 were used to select lines of strong output in pulsed lasers. Care was employed to ensure that all known atmospheric absorbers were included for these lines.

TABLE I

PULSED DF LASER TRANSITIONS

Laser Line Identification	Laser Frequency (cm^{-1})	Relative Energy*
2P (8)	2631.09	2.37
2P (9)	2605.87	2.68
2P (10)	2580.16	4.24
2P (11)	2553.97	3.46
3P (8)	2546.37	2.74
3P (9)	2521.81	5.38
3P (10)	2496.61	3.35
3P (11)	2471.34	2.26

*Energy of 1P (10) transition is taken as 1.

B. SELECTION OF ATMOSPHERIC ABSORBERS AND ABSORPTION COEFFICIENTS FOR DF LASER LINES

The atmospheric absorbers of importance at DF laser wavelengths are N_2O, CH_4, H_2O, HDO and CO_2. This is confirmed by both absorption cell experiments[3] and theoretical calculations based on experimental data.[4] Reference 4 is an Air Force Cambridge Research Laboratory (AFCRL) compilation of the molecular spectroscopic parameters for a number of infrared-active molecules (including those listed above) which occur naturally in the terrestrial atmosphere. Parameters included in the compilation for each absorption line are: frequency, intensity, half-width, energy of the lower state of the transition, vibration and rotational identifications of the upper and lower energy states, an isotopic identification, and a molecule identification. We have written a code which sorts the AFCRL data according to absorbing molecules and vibrational transition over a given frequency interval and calculates the absorption cross section for the absorbing molecule at the laser frequency of interest.

The sea level absorption cross sections used for the atmospheric absorbers at DF laser frequencies are given in Table II. The absorption by N_2 on the collision induced vibrational continuum band centered around 4.3 μ is not included here, but is a well documented phenomenon. Calculations indicate that the N_2 continuum is a strong absorber at the longest wavelengths at sea level. Following McClatchy[4] the effect of absorption due to the water continuum was not included. This effect will be investigated in a later phase of this effort. At higher altitudes the cross sections are reduced according to the appropriate pressure dependence. The temperature dependence is not included at this time. (See Section III, RESULTS.)

The N_2O cross sections computed are in excellent agreement with the absorption cell measurements of Ref. 3 for all the laser transitions considered. For CH_4 the agreement between these cross sections and the absorption cell measurements of Ref. 3 are not as good. In all cases we have used the cross sections computed from the AFCRL data, which average about a factor of 3 to 4 lower than the absorption cell measurements. The effects of any errors thus introduced on the calculated atmospheric temperature rise are small, because in no case is CH_4 the major absorber. For CO_2, where the absorption is due to lines of the 4.3 μ band (hundreds of wave numbers removed from the laser frequency) we have used the experimental results of Ref. 3. These fall between the values calculated form the AFCRL data using a Lorentz line shape (higher than Ref. 3) and the best experimental line shape fit to CO_2 absorption data[6] (lower than Ref. 3).

The absorption cross section is calculated from the integrated absorption coefficient assuming a Lorentz line shape using the relation:

$$\sigma = \frac{S}{\pi} \frac{\Delta\nu}{(\nu - \nu_o)^2 + \Delta\nu^2} \qquad (1)$$

TABLE II

SEA LEVEL ABSORPTION CROSS SECTIONS AT
DF LASER WAVELENGTHS
(cm^2/molecule)

DF Laser Line	N_2O	HDO	H_2O	CH_4	CO_2
2P (11)	1.0^{-20}	3.7×10^{-23}	8.0×10^{-29}	-	-
2P (10)	2.9^{-20}	1.77^{-22}	1.4×10^{-28}	-	-
2P (9)	3.57^{-22}	1.53^{-21}	1.0×10^{-27}	1.5^{-23}	-
2P (8)	-	5.0^{-22}	6.8^{-26}	2.0^{-22}	-
3P (11)	4.2^{-21}	6.7×10^{-23}	1.1^{-25}	-	1.4^{-23}
3P (10)	2.39^{-22}	3×10^{-24}	9.3^{-26}	-	6.5^{-24}
3P (9)	4.7^{-22}	1.2×10^{-23}	8.0×10^{-28}	-	3.15^{-24}
3P (8)	2.9^{-20}	5.7×10^{-23}	7.4×10^{-28}	2.5^{-22}	-

where σ is the cross section in cm^2/particle, S (the integrated absorption cross section cm^{-1}/particle-cm^{-2}) = $\int \sigma(\nu)\, d\nu$, $\Delta\nu$ is the half-width in cm^{-1} and $(\nu - \nu_o)$ is the difference in wave number between the laser line frequency and the center of the absorbing line. This procedure gives too high a value for CO_2, since CO_2 is known to be sub-Lorentzian far from line center. Reference 6 reports measurements of CO_2 absorption both in pure CO_2 and in mixtures of CO_2 with N_2 and O_2. The absorption due to the wings of the strong lines in the ν_3 band centered at 2349 cm^{-1} is much less than that calculated with the Lorentz shape. The data in N_2 and O_2 are fit(6) with the following equation, which retains the Lorentz pressure dependence but requires a nearly exponential modification of the frequency dependence.

$$\sigma = \frac{S}{\pi} \frac{\Delta\nu}{(\nu - \nu_o)^2 + \Delta\nu^2} e^{-0.46\,(|\nu - \nu_o| - 5)^{0.46}} \qquad (2)$$

Use of this relation gives values for CO_2 absorption cross sections at the DF laser frequencies of interest which are lower than those of Ref. 3. The cross sections for CO_2 given in Table II are consistent with the measurements in Ref. 3. It should be noted that any errors introduced by uncertainties in the value of the CO_2 cross sections would be significant only at high altitudes where CO_2 becomes a significant absorber (see Fig. 14). At sea level CO_2 is only a very minor contributor to the atmospheric temperature rise.

For atmospheric water vapor the situation is complicated by the fact that both H_2O and HDO are absorbers, with HDO such a strong absorber that it is significant even in its natural isotopic abundance of 300 ppm of H_2O. The calculated cross sections for H_2O and HDO obtained from the AFCRL data and the experimental results of Ref. 3 are in sharp disagreement for individual laser lines. Because the experimental absorption cross sections were obtained by subtracting the very large absorption due to D_2O from the measured absorption, we have rather arbitrarily assumed the error to be in the experiment and have chosen to use the values calculated from the AFCRL data which for H_2O are in agreement with data of Bates.(7) It turns out that, when the laser power is evenly distributed over all the laser lines with equal powers, either set of cross section values gives the same temperature rise. This is because the sum over all lines of the absorption cross sections for HDO-H_2O happens to be the same for both the AFCRL and Ref. 3 cases. It should be noted, however, that for individual laser lines the values are very different and that any calculations of the temperature rise due to H_2O-HDO, which use less than all of the eight laser lines of Table I or employ different power levels on the lines, may be sensitive to which set of cross section values is chosen.

C. SELECTION OF CO LASER LINES

In contrast to DF chemical lasers, the CO molecules in electric CO lasers are first excited to relatively low vibrational levels by the discharge. They are then pumped to rather high vibrational levels by intermolcular V-V transfer processes. Due to anharmonic effects the vibrational distribution function is generally strongly distorted from a Boltzmann distribution in a manner which favors the higher vibrational levels. As a result, the highest gain is usually observed in relatively high levels (typically $7 \lesssim \nu \lesssim 15$). Recently, lasing has been observed on the lower levels (down to the 1-0 transition) in high gain-low loss systems.

As we shall see, the higher vibrational levels which emit at longer wavelengths, are more strongly absorbed by the H_2O (ν_2) 6.3-μ band. In addition, the kinetics of the lower levels take place more rapidly, offering the possibility of greater specific power. For these reasons it may be desirable to suppress lasing on the high vibrational levels (with a grating or passive H_2O absorber, for example) and force lasing on the low vibrational levels. Experiments to demonstrate the feasibility of this are currently underway at AERL.

To assess the relative advantages of low and high vibrational levels it is necessary to consider a wide range of transitions. The positions of the CO laser lines used in calculating the results presented here are given in Table III together with absorption coefficients and cross sections for absorption by H_2O, the only important absorber. The wavenumber positions for CO, listed in Table III, were calculated from spectroscopic constants given by Mantz.[8a, b] These should be good to ± 0.01 cm^{-1}. The wavenumbers agree well with those used by Long[9] and McClatchy.[10]

D. SELECTION OF CO ATMOSPHERIC ABSORBERS AND ABSORPTION COEFFICIENTS

Survey calculations were made of absorption of CO laser lines by H_2O, CO_2, O_3, N_2O and CH_4. Compared with H_2O, the absorption of O_3, N_2O and CH_4 was negligible. The absorption of the 6P (9) CO line at 1977.28 cm^{-1} by CO_2 was also negligible. For the 2P (9) CO line at 2081.26 cm^{-1}, the CO_2 absorption was down from that due to H_2O by a factor of 6. (The sub-Lorentz CO_2 line contour of Winters, et al.,[6] was used.) In the remainder of this work we concern ourselves only with absorption by H_2O.

Extensive calculations of absorption of CO laser radiation by atmospheric H_2O have been made by McClatchey.[10, 11] However, this work has two limitations. First, the Lorentz contour, Eq. (1) was used for the H_2O spectral absorption coefficient. The experiments of Long, et al.,[9] show that the absorption of CO laser lines in the wings of H_2O lines is typically 40% greater than given by Eq. (1). To fit their data they

TABLE III

POSITIONS OF CO LASER LINES AND ABSORPTION COEFFICIENTS AND CROSS SECTIONS FOR H_2O ABSORPTION

Laser Line	ν (cm^{-1})	k for p_{H_2O} = 5.8 torr (km^{-1})* Present	Ref. 10	$(10^{-24}\sigma\ cm^2)$ Present
2P (8)	2085.343	0.090	0.065	4.7
2P (9)	2081.285	0.080	0.052	4.2
2P (15)	2056.047	0.096	0.038	5.1
3P (10)	2051.075	0.171	0.108	9.0
3P (15)	2030.158	0.132	0.063	7.0
3P (16)	2025.875	0.46	0.030	24.0
4P (8)	2033.143	0.133	0.038	7.0
4P (9)	2029.128	0.137	0.049	7.2
4P (15)	2004.337	0.21	0.072	11.0
5P (9)	2003.167	0.24	0.088	12.6
6P (9)	1977.277	0.29	0.130	15.3
6P (10)	1973.299	0.32	0.117	17.0

*$k = \sigma N \times 10^5$ where σ is cross section/particle in cm^2 and N is number density in particles/cc.

assumed that the absorption coefficient follows the Lorentz contour for $|\nu - \nu_o| \leq \nu_m$, but that outside this range it is given by

$$\sigma(\nu) = \frac{S}{\pi} \frac{(\nu_m)^2 \Delta\nu}{\left[(\nu_m)^2 + \Delta\nu^2\right] |\nu - \nu_o|^m}, \quad |\nu - \nu_o| \geq \nu_m \tag{3}$$

Equations (1) and (3) agree at $|\nu - \nu_o| = \nu_m$. The best fit was obtained using $\nu_m = 3\,\Delta\nu$ and $m = 1.77$.

McClatchey and Long considered absorption by H_2O lines whose centers lie within 20 or 25 cm^{-1}, respectively, of the CO laser line. This amounts to a cut-off: $\sigma(\nu) = 0$, $\nu > \nu_{max}$ or $\nu < \nu_{min}$. However, we find by allowing $\nu_{min} = \nu_o - 350\ cm^{-1}$, that in some cases half the absorption is due to lines 150 cm^{-1} distant. The true contour in the far wings of H_2O lines cannot be determined from the available data. Unfortunately, H_2O does not form sharp band heads as does CO_2, whose far wing line profile may be determined more reliably. We consider extrapolation of Eq. (3) less arbitrary than cutting it off. Using the extended line profile we find that Long's data may be fitted using $\nu_m = 3\,\Delta\nu$ and $m \sim 1.88$. Values of m for various individual lines ranged from 1.85 to 1.91.)

In mixtures of water vapor and air the H_2O half-width is given by

$$\Delta\nu = a_o p_t [1 + (B-1)\chi] \tag{4}$$

where a_o is the half-width per atmosphere of air, p_t is the total pressure in atmospheres, χ is the mole fraction of H_2O in the mixture and B is the self-broadening coefficient. Long, et al.,[9] find B = 8 to 27. We used the value B = 5 from Ref. 12. The difference is insignificant because $\chi < 0.01$ in cases of interest.

Our results are presented in Table III. Equation (3) was used with $\nu_m = 3\Delta\nu$ and $m = 1.88$. The cut-offs were $\nu_{min} = \nu_o - 350\ cm^{-1}$ and $\nu_{max} = \nu_o + 50\ cm^{-1}$. (Absorption at larger wavenumbers, farther away from the center of the 6.3-μ H_2O band is negligible.) The absorption coefficients are larger than those scaled from McClatchey's calculations[10] for $p_{H_2O} = 3.3$ torr (mid-latitude winter case), due to the use of the "super-Lorentz" profile and its extension farther into the wings of the H_2O lines. There are no Ohio State[9] experimental or theoretical results for many of these lines. Their work has generally been on lines at smaller wavenumbers (higher CO vibrational levels) located nearer the center of the 6.3-μ band of H_2O, for which the attenuation coefficients are typically larger.

Table III shows the cross sections we have used for water based on the above discussion. For comparison we have shown the differences between our results and those of McClatchey[10] in terms of absorption coefficients. (Note added in proof: A recent work[13] reports absorption coefficients in good agreement with the present ones.)

II. KINETICS OF ABSORPTION OF DF AND CO LASER RADIATION

The absorption of DF laser radiation is complicated by the number of atmospheric species which absorb this radiation and by the fact that the upper level of the absorbing transition is frequently a high-lying vibrational level, as in N_2O and CH_4. Thus, to describe the absorption kinetics it is necessary to include a large number of levels. A complete diagram of all the important vibrational levels of the atmospheric species important for DF and CO absorption kinetics is shown in Fig. 1. It is important to keep in mind that each vibrational level shown actually consists of a manifold of vibration-rotation states.

A. Rotational Relaxation

Because of the large number of levels, it is necessary to make approximations in which groups of levels are lumped together and treated as a single level. To begin with, it will be assumed that all the rotational levels belonging to a given vibrational level remain in equilibrium with one another at the translational temperature T. This assumption will be valid if the rotational relaxation time τ_R is short compared with the time for a radiatively induced transition, that is, if

$$\Phi_\nu \ \sigma_\nu \ \tau_R \ll 1, \tag{5}$$

where Φ_ν is the flux of laser photons, and σ_ν is the absorption cross section. Both the rotational relaxation time and the absorption cross section depend upon the pressure through the molecular collision frequency ν_c. Thus, the adequacy of assumption (5) will depend on the pressure. For a purely Lorentz broadened line, the cross section at the frequency ν is given by Eq. (1). The line half-width $\Delta\nu$ is proportional to the pressure and may be represented by the relation

$$\Delta\nu = a\,p,$$

where p is the pressure.

The rotational relaxation time is more difficult to quantify precisely. Since rotational relaxation involves a great many levels, it is inevitably a complex process. For example, an extremely short laser pulse (shorter than the time between molecular collisions) will affect only molecules in specific quantum states. The population of the perturbed states will then

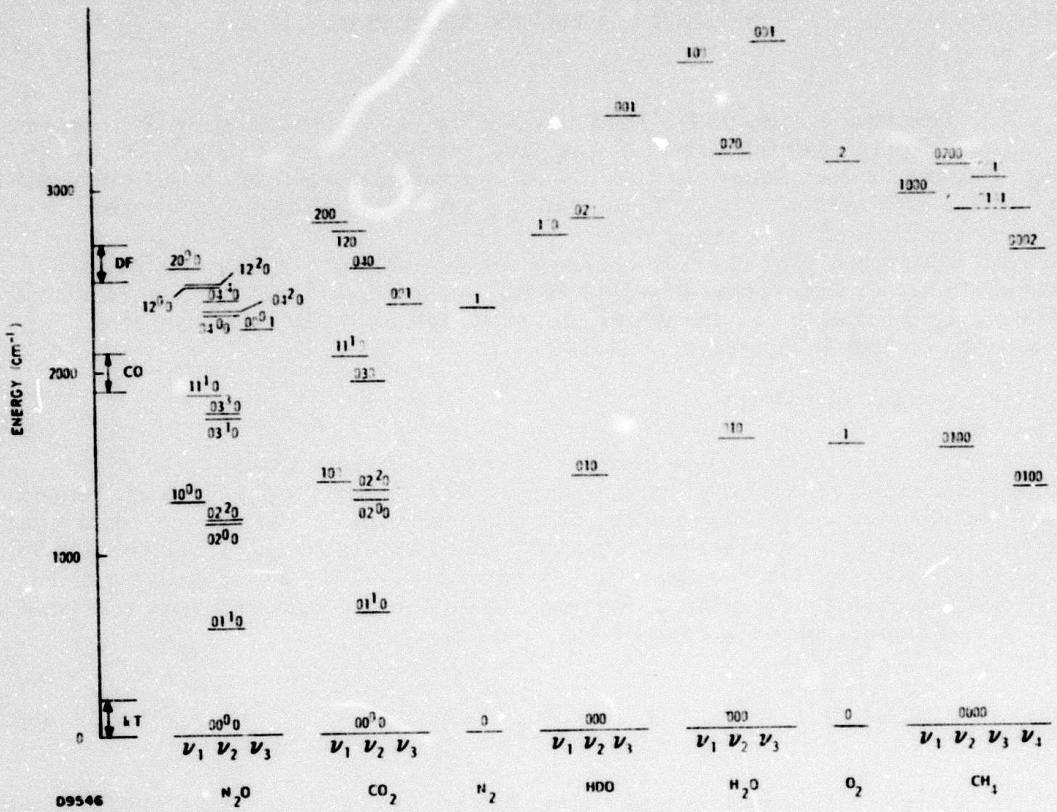

Fig. 1 Vibrational Energy Level Diagram for DF and CO Laser Atmospheric Absorption Kinetics

relax by reorientation of the remaining molecules having the same total angular momentum and by transitions from nearby rotational energy levels. The appropriate relaxation time for this case corresponds to the gain relaxation time measured following a Q-switched laser pulse.[14] Longer laser pulses will pertrub the populations of all the rotational levels around the level from which the transition originates; in this case the time for the system to relax to equilibrium will be considerably longer. Moreover, experimental evidence indicates that the thermally averaged relaxation time (measured acoustically) may correspond to as small as a few collisions or as large as 30 collisions or more (for rotationally light molecules, such as HCl, at elevated temperatures).[15] Moreover, it has been found both theoretically and experimentally that for molecules in high rotational levels the rotational relaxation time increases exponentially with rotational energy.[16]

To examine the importance of rotational relaxation it is convenient to express the relaxation time in the form

$$p\tau_R = \beta, \tag{6}$$

where β is independent of pressure. Equation (4) may then be expressed

$$\Phi_\nu \sigma_\nu \tau_R = \Phi_\nu \frac{\alpha\beta}{\pi} \frac{S}{(\nu - \nu_o)^2 + (\alpha p)^2} \ll 1. \tag{7}$$

When the laser line lies in the wing of the absorber ($|\nu - \nu_o|/\alpha p \gg 1$) we obtain the inequality

$$\Phi_\nu \ll \frac{\pi (\nu - \nu_o)^2}{\alpha\beta S} . \tag{8}$$

The right-hand side is a function only of the laser frequency and the absorbing level, and is independent of the pressure. The limiting fluxes for the most important DF laser lines, calculated using this expression, are summarized in Table IV. At sufficiently high pressures ($\alpha p/|\nu - \nu_o| \gg 1$) the laser line will lie within the Lorentz width of the absorber. The limiting flux Φ_ν will then increase as p^2. At sufficiently low pressures, of course, the line will become Doppler broadened and the cross section σ_ν will be independent of pressure. The limiting flux Φ_ν at which rotational relaxation becomes important will then be proportional to the pressure; at a sufficiently low pressure rotational relaxation will always become important. However, as shown in Table IV, this occurs only at very low pressures ($\lesssim 0.01$ atm).

When rotational relaxation becomes important the atmosphere will begin to "bleach", that is, molecules will be removed from the absorbing level and deposited in the upper level faster than they can be relaxed by collisions and the atmosphere will become transparent. Thus, by ignoring

TABLE IV

DF LASER INTENSITY AT WHICH ROTATIONAL RELAXATION BECOMES IMPORTANT

DF Laser Transition	Absorbing Species	Relaxation Time (collisions)	Laser Intensity (W/cm^2)	Pressure Range (atm)
2P (8)	CH_4	10	8×10^9	$0.01 < p < 0.2$
2P (10)	N_2O	2	4×10^9	$0 < p < 1$
2P (11)	N_2O	2	1×10^{10}	$0 < p < 3$
3P (8)	N_2O	2	1×10^9	$0.02 < p < 0.04$

Notes:

At lower pressures the absorbing lines become Doppler broadened, and the intensity at which rotational relaxation becomes important decreases linearly with the pressure. At higher pressures the laser line falls within the Lorentz width of the absorbing line and the intensity at which rotational relaxation becomes important increases as the square of the pressure.

Laser transitions and absorbing species not indicated in Table IV show no rotational relaxation effects at laser intensities below 10^{10} W/cm^2.

rotational relaxation we place an upper bound on the extent of absorption. The results shown in Table IV indicate that rotational bleaching should not be important for DF laser intensity levels below 10^{10} W/cm^2. Although a few isolated lines may be bleached at this power level, their contribution to the total absorption on the vibrational bands to which they belong will not be significant. It should be emphasized, however, that this result cannot be simply extrapolated to all IR lasers. All the important absorbers for DF radiation have rather small absorption cross sections because either the absorbing bands correspond to vibrational overtones, (as in the case of N_2O and CH_4), or the laser line lies in the far wings of the absorbing line (as in CO_2), or the rotational structure of the band reduces the contribution of individual lines (as in HDO and H_2O). For laser lines overlapped by strong absorbing lines, rotational relaxation may become important.

B. VIBRATIONAL RELAXATION

Even if rotational equilibrium is assumed, there remain a great many vibrational levels of importance for the absorption kinetics, as indicated in Fig. 1. Although it is not difficult to handle this number of levels on the computer, it is appropriate to make some further simplifications since there do not exist enough kinetic rate data to enable one to describe the system in complete detail. The kinetics of the important atmospheric absorbers are discussed in the following sections.

1. Kinetics of Absorption of DF Laser Radiation by N_2

DF laser radiation is absorbed by N_2 on the collision induced vibrational continuum band centered around 4.3 μ:

$$N_2 (v = 0) + h\nu + M \rightarrow N_2 (v = 1) + M + \Delta E. \qquad (9)$$

The excess energy $\Delta E = h\nu - E_{vib} \sim 250$ cm^{-1} appears immediately as translational and rotational heating of the N_2 and M molecules.

The relaxation of N_2 (v = 1) by the dominant atmospheric species (N_2, O_2, H_2O) has been extensively studied as a result of interest in the CO_2 - N_2 laser.[17] T-V deactivation of N_2 (v = 1) by N_2 and O_2 and V-V transfer to O_2 are extremely slow. The most important relaxation path is provided by H_2O. It has not been established directly whether the quenching of N_2 by H_2O proceeds by a T-V (or vibration to rotation) process, or by V-V transfer to the ν_2 mode of H_2O,

$$N_2 (v = 1) + H_2O (000) \rightarrow N_2 (v = 0) + H_2O (010) + 735 \text{ cm}^{-1}. \qquad (10)$$

However, the subsequent relaxation of H_2O (010) is so fast that for practical purposes it does not matter.

These processes are summarized in Fig. 2. The time scales for the various processes in this and the following sections are based on an atmosphere composed of

$$N_2 \ (2 \times 10^{19} \text{ molecules/cm}^3),$$

$$O_2 \ (5 \times 10^{18} \text{ molecules/cm}^3),$$

$$H_2O \ (3 \times 10^{17} \text{ molecules/cm}^3),$$

at a temperature of 300°K. The amount of energy which appears as thermal (translational + rotational) energy at each step is also indicated. We see that under the above conditions, absorption on the N_2 continuum band results in a small amount of essentially instantaneous heating followed by slow heating on the N_2 relaxation time scale, which is on the order of 8×10^{-4}s.

2. Kinetics of Absorption of DF Laser Radiation by CO_2

DF laser radiation is absorbed by CO_2 on the ν_3 fundamental band centered at 4.3 μ.

$$CO_2 \ (000) + h\nu \rightarrow CO_2 \ (001) + \Delta E. \qquad (11)$$

The absorption takes place principally in the far wings of the lines corresponding to low, thermally populated, rotational levels. Thus most of the excess energy ΔE (~ 250 cm^{-1}) appears instantaneously as translational energy of the CO_2 and collisional broadening molecules.

The relaxation of CO_2 (001) by the dominant atmospheric species (N_2, O_2, H_2O) has been extensively studied as a result of interest in the CO_2 - N_2 laser.[17] Relaxation takes place principally via intermolecular V-V transfer to N_2.

$$CO_2 \ (001) + N_2 \ (v = 0) \rightarrow CO_2 \ (000) + N_2 \ (v = 1) - 18 \text{ cm}^{-1} \qquad (12)$$

The subsequent relaxation of N_2 (v = 1) is described above.

These processes are summarized in Fig. 3, where the relaxation times correspond to the same atmospheric conditions as in Fig. 2. Aside from the small amount of heat released by the absorption process, the overwhelming effect of absorption by CO_2 is to heat the gas on a slow time scale ($\sim 10^{-3}$s) corresponding to the relaxation of the N_2 (v = 1) level.

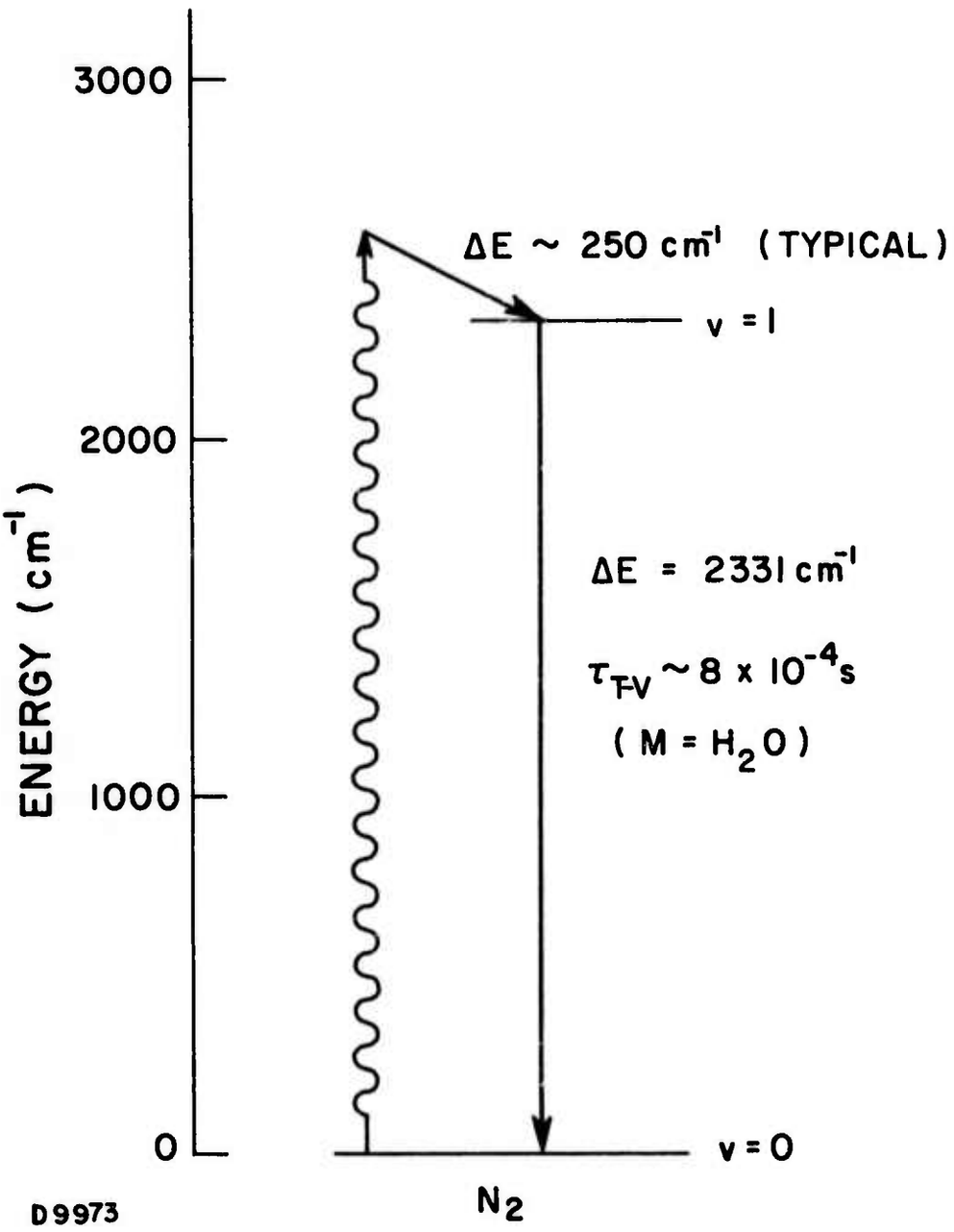

Fig. 2 Kinetics of Absorption of DF Laser Radiation by N_2

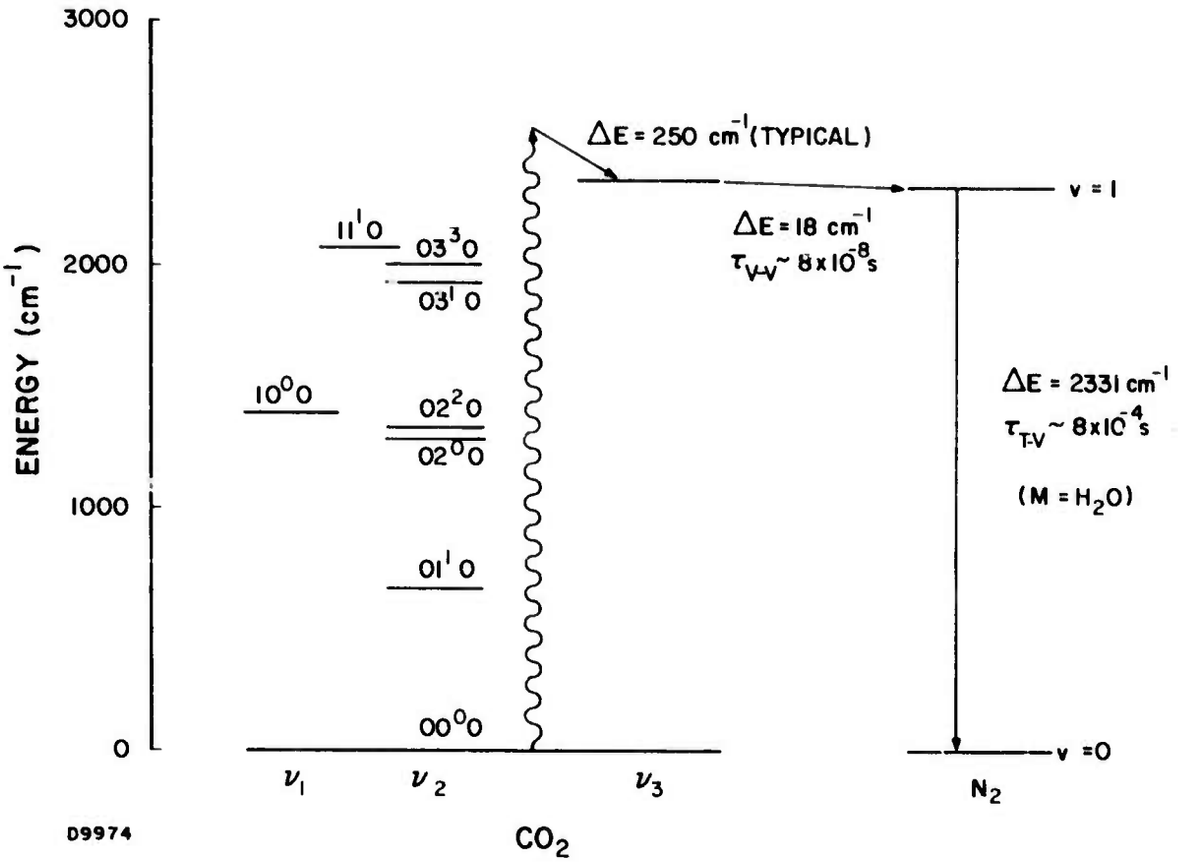

Fig. 3 Kinetics of Absorption of DF Laser Radiation by CO_2

3. Kinetics of Absorption of CO and DF Laser Radiation by H_2O

CO laser radiation is absorbed by H_2O on the ν_2 fundamental transition,

$$H_2O\ (000) + h\nu \rightarrow H_2O\ (010) + \Delta E. \qquad (13)$$

The excess energy ($\Delta E \sim 400\ cm^{-1}$) appears as translational and rotational energy of the H_2O molecule, and is assumed to be thermalized instantly.

The absorption of DF radiation by H_2O, while somewhat controversial, as mentioned above, is alleged to occur on the same vibrational transition. The relatively large excess energy ($\Delta E \sim 900\ cm^{-1}$ for DF lasers) appears as translational and rotational energy of the H_2O molecule, and is presumed to be thermalized instantaneously.

The relaxation of the H_2O (ν_2) mode has been studied experimentally for a long time, and while considerable uncertainty remains for some of the important rates, a broad understanding is possible.[17] The most important processes for the relaxation of H_2O (ν_2) are near resonant V-V transfer to O_2,

$$H_2O\ (010) + O_2\ (v = 0) \rightarrow H_2O\ (000) + O_2\ (v = 1) + 38\ cm^{-1}, \qquad (14)$$

and T-V quenching,

$$H_2O\ (010) + M \rightarrow H_2O\ (000) + M + 1595\ cm^{-1}, \qquad (15)$$

where M = N_2, O_2, and (most importantly) H_2O itself. There is considerable scatter in the data on the T-V quenching of H_2O (ν_2) by H_2O, but the rate is apparently quite fast, on the order of $(2 \times 10^{-12}) - (5 \times 10^{-11})\ cm^3/s$, (about 10 to 100 collisions). The most recent data favor the fastest rate. The data on V-V transfer to O_2 (reaction (14)) are somewhat confused due to apparent errors in most of the papers. The correct rate seems to be about $1.5 \times 10^{-12}\ cm^3/s$. The energy which is transferred to O_2 relaxes relatively slowly by T-V quenching of O_2 by H_2O,

$$O_2\ (v = 1) + H_2O\ (000) \rightarrow O_2\ (v = 0) + H_2O\ (000) + 1556\ cm^{-1}, \qquad (16)$$

and by transfer back to H_2O followed by quenching of the H_2O.

These processes are summarized in Fig. 4, where the times indicated correspond to the atmospheric conditions of Figs. 2 and 3. The absorption of a laser photon leads to some immediate heating (for a time on the order of the rotational relaxation time) as indicated. T-V quenching of the H_2O leads to further very rapid heating (with a time scale on the order of 10^{-7} to 10^{-6}s. The energy that is transferred to O_2 produces heating on a somewhat larger time scale, on the order of 10^{-5}s. The extent of heating occurring on the fast and slow time scales depends on the relative rates of T-V quenching and V-V transfer to O_2. If the faster H_2O/O_2 V-V transfer rate and/or slower H_2O/H_2O T-V quenching rate is correct, or if the humidity is low (as it will surely be at higher altitudes) then the bulk of the H_2O vibrational energy will be transferred to O_2. This will shift the heating to significantly longer times. These uncertainties become even more important for the absorption of CO laser radiation, since $H_2O(\nu_2)$ is the dominant absorber.

4. Kinetics of Absorption of DF Laser Radiation by N_2O

DF laser radiation is absorbed by N_2O principally on the ν_2 overtone transition,

$$N_2O\,(00^00) + h\nu \rightarrow N_2O\,(20^00) + \Delta E \qquad (17)$$

and the combination band transition

$$N_2O\,(00^00) + h\nu \rightarrow N_2O\,(12^{\ell}0) + \Delta E \qquad (18)$$

A small amount of absorption takes place on the corresponding transitions from the $N_2O\,(01^10)$ level, but this may be ignored.

Most of the available data on N_2O vibrational relaxation[18-21] were obtained in pure N_2O and N_2O/N_2 mixtures, and do not shed much light on the most important processes in the atmosphere. To identify the most important processes we note that N_2O is very similar to CO_2. Both are linear triatomic molecules with comparable masses. It is important to note, however, that mode ν_1 is IR active (that is, it possesses a dipole moment) in N_2O, whereas it is not IR active in CO_2. This is because CO_2 is a symmetric molecule whereas N_2O is not, having the configuration N-N-O. It is also important to remember that the levels 10^00 and 02^00 are strongly coupled by Fermi resonance in CO_2 but not in N_2O. Available data indicate that modes ν_1 and ν_2 of CO_2 are rapidly coupled by collisions and may be assumed to relax together, but that mode ν_3 is only weakly coupled to the other two and relaxes by itself. All the data concern mixtures rich in CO_2, so that modes ν_1 and ν_2 may be coupled by <u>intermolecular</u> V-V transfer processes of the type

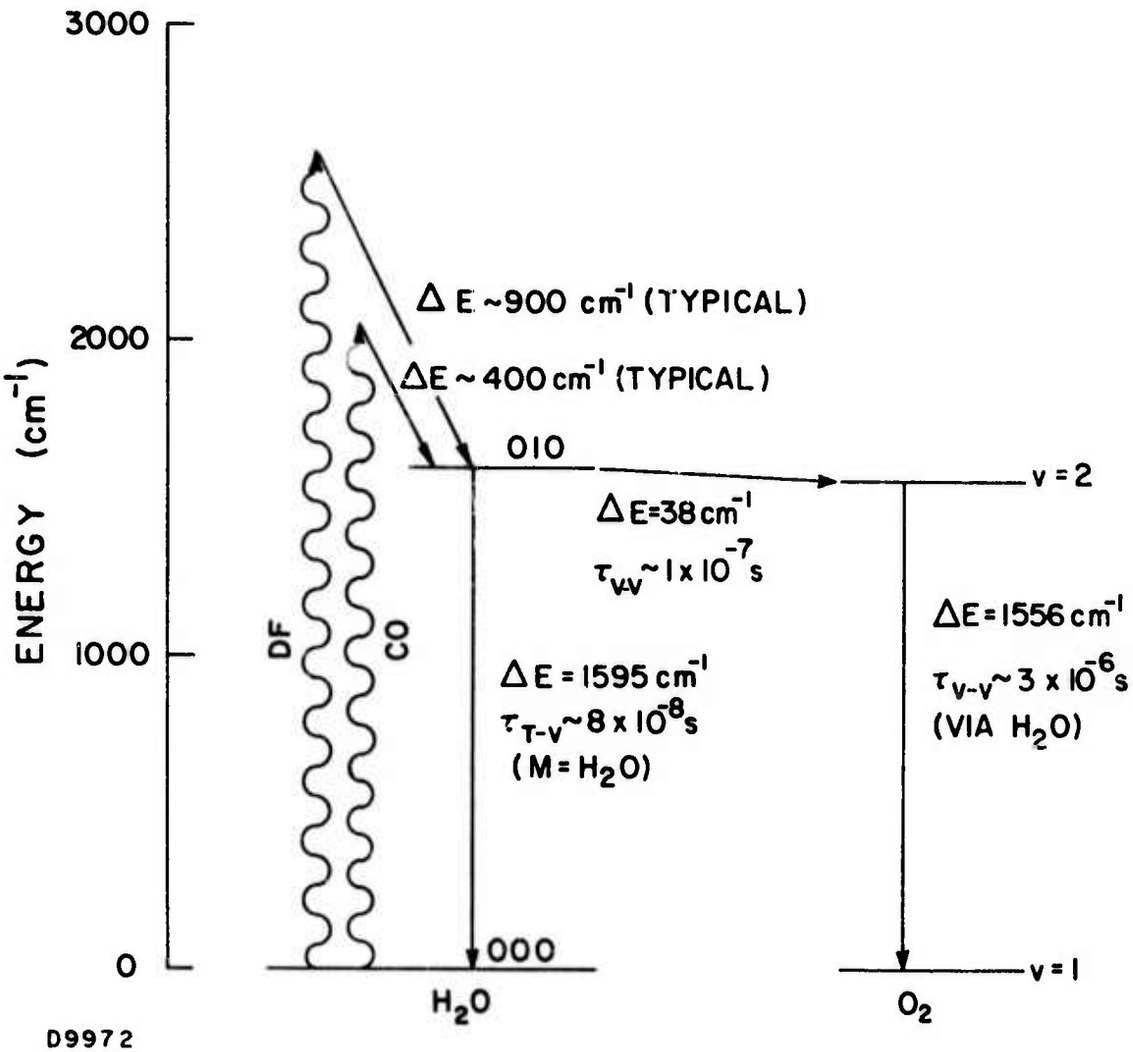

Fig. 4 Kinetics of Absorption of CO and DF Laser Radiation by H_2O

$$CO_2\,(10^00) + CO_2\,(00^00) \rightarrow 2\,CO_2\,(01^10)$$
$$\text{or} \rightarrow CO_2\,(00^00) + CO_2\,(02^{\ell}0). \qquad (19)$$

It has also been suggested[22-23] that in dilute mixtures coupling via <u>intromolecular</u> processes,

$$CO_2\,(10^00) + M \rightarrow CO_2\,(02^{\ell}0) + M \qquad (20)$$

where M = CO_2, is rapid due to the Fermi resonance which mixes the levels (10^00) and (02^00).

There is no corresponding evidence of rapid coupling of modes ν_1 and ν_2 of N_2O in the atmosphere. Intermolecular V-V processes similar to (19) are unimportant due to the high dilution, and modes ν_1 and ν_2 are not mixed by Fermi resonance. The acoustical data have been interpreted in terms of the simultaneous relaxation of modes ν_1 and ν_2, but the data are not compelling. For lack of evidence we shall make the same approximation.

The evidence does show, however, that mode ν_3 is only weakly coupled to modes ν_1 and ν_2. Results obtained in N_2O/N_2 mixtures indicate that quenching of mode ν_3 by N_2 requires about 10^5 collisions, which is only about a factor of two faster than the corresponding process in CO_2. It is not known to which level the CO_2 (00^01) level is quenched, although the data of Cannemijer[24] indicate that it is the CO_2 $(03^{\ell}0)$ level in CO_2-CO_2 collisions and the CO_2 $(02^{\ell}0)$ level in CO_2-rare gas collisions. However, even if it is the near-resonant $04^{\ell}0$ or other nearby levels in N_2O, detailed balance indicates that the reverse rate, coupling modes ν_1 and ν_2 to mode ν_3 in collisions with N_2, will be slow. This is supported by the experiments of Yardley,[21] who excites N_2O mode ν_3 in mixtures with N_2. He observes that N_2O mode ν_3 rapidly couples to N_2 by V-V transfer in about 1100 collisions. However, at the end of this (short) time the extent of residual excitation in mode ν_3 indicates that modes ν_1 and ν_2 have not been excited by either direct intramolecular V-V processes or intermolecular V-V transfer back from N_2.[25] Quenching of CO_2^* (ν_3) to modes ν_1 and ν_2 by H_2O is much faster than by N_2, requiring on the order of 10^3 collisions. This probably because H_2O rotation can absorb much of the nonresonance between CO_2 (00^01) and CO_2 $(mn^{\ell}0)$. However, even this rate of coupling is likely to be much slower than direct quenching of modes ν_1 and ν_2 by H_2O (see below).

We are therefore led to neglect the coupling of modes ν_1 and ν_2 to mode ν_3 and to assume that modes ν_1 and ν_2 are rapidly coupled. This leads to the model shown in Fig. 5. According to this model, modes ν_1 and ν_2 are reduced to four lumped levels, each consisting of several near-resonant levels as indicated by the dotted lines.

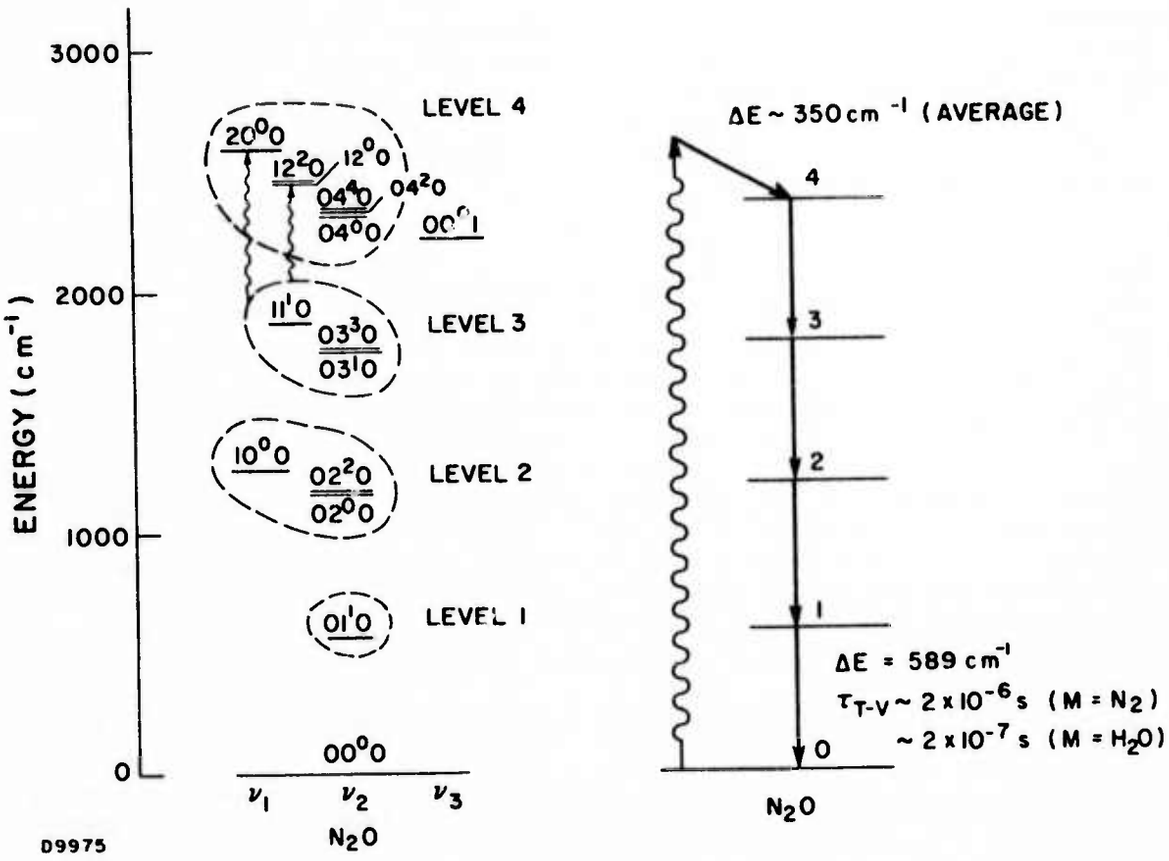

Fig. 5 Kinetics of Absorption of DF Laser Radiation by N_2O

Few of the rates of relaxation of these levels have been measured experimentally. The relaxation of the $N_2O(\nu_2)$ model has been determined by acoustical and spectrophonic techniques[18] and found to be 1.8×10^{-14} cm^3/s. This is approximately a factor of five faster than the corresponding relaxation rate for $CO_2(\nu_2)$, as might be expected from the slightly lower vibrational frequency of $N_2O(\nu_2)$. To scale the rate to different temperatures we assume that the temperature dependence for $N_2O(\nu_2) + N_2$ is the same as that for $CO_2(\nu_2) + N_2$. To scale the rate to higher levels we assume the harmonic oscillator rule, which says that for level $(0\ m^{\ell}0)$ the quenching rate is proportional to m.

Continuing the analogy to CO_2, we anticipate that the quenching of $N_2O(\nu_2)$ by H_2O should be a very rapid process since the quenching of $CO_2(\nu_2)$ requires only about 20 collisions.[17] Two theories have been advanced to explain the rapid quenching of CO_2. Widom and Bauer[26] suggest that CO_2 and H_2O interact chemically, since H_2CO_3 is known to exist in solution. Semiquantitative calculations based on this mechanism give the right order of magnitude for the quenching rate. Sharma[27] suggests that the multipolar interaction between CO_2 and H_2O is responsible. Detailed computations based on this mechanism are also in reasonable agreement with the experimental data. If the latter explanation is correct, a similar mechanism should operate in N_2O-H_2O collisions. On this basis we assume that the rate of quenching of N_2O (01^10) by H_2O is the same as the measured rate of quenching of CO_2 (01^10) by H_2O at all temperatures. To scale to higher levels, the harmonic oscillator rule is used.

The quenching of $N_2O(\nu_1)$ is likely to be much slower because of the larger vibrational level spacing, compared with mode ν_2. Provided that modes ν_1 and ν_2 are closely coupled the direct quenching of mode ν_1 can be ignored. However, if they are not so coupled it is necessary to consider what might be the most important processes relaxing mode ν_1. A strong candidate for the dominant role is near-resonant V-V transfer to H_2O.

$$N_2O\ (10^00) + H_2O\ (000) \rightarrow N_2O\ (00^00) + H_2O\ (010) - 310\ cm^{-1} \quad (21)$$

Although this reaction might seem far from resonant, H_2O has shown itself capable of a variety of not-so-resonant processes, apparently because a large amount of nonresonance can be made up by the H_2O rotational frequency. Similar reactions to which (21) may be compared include the reactions

$$CS\ (v = 1) + H_2O\ (000) \rightarrow CS\ (v = 0) + H_2O\ (010) - 323\ cm^{-1}, \quad (22)$$

$$NO\ (v = 1) + H_2O\ (000) \rightarrow NO\ (v = 0) + H_2O\ (010) + 281\ cm^{-1}, \quad (23)$$

$$N_2O\ (00^01) + HBr\ (v = 0) \rightarrow N_2O\ (00^00) + HBr\ (v = 1) - 335\ cm^{-1} \quad (24)$$

These reactions have room temperature rates (in the exothermic direction) equal to 1×10^{-11}, 2×10^{-12}, and 2×10^{-12} cm^3/s, respectively.[17] A rate equal to 10^{-12} cm^3/sec seems reasonable for reaction (21) in the exothermic direction. This is much slower than the quenching of mode ν_2 by H_2O and will be negligible if the modes are coupled. However, if modes ν_1 and ν_2 are not coupled, their rates of relaxation are likely to be quite different.

These processes were summarized in Fig. 5, where the times indicated correspond to the atmospheric conditions of Figs. 2, 3, and 4. Only a small amount of heating accompanies the absorption of a laser photon. The bulk of the heating occurs on a time scale of the order of 2×10^{-7}s, corresponding to the quenching of N_2O (ν_2) by H_2O.

5. Kinetics of Absorption of DF Laser Radiation by CH_4

DF laser radiation is absorbed by CH_4 on the ν_4 overtone band

$$CH_4\ (0000) + h\nu \rightarrow CH_4\ (0002) + \Delta E, \tag{25}$$

and the combination band

$$CH_4\ (0000) + h\nu \rightarrow CH_4\ (0101) + \Delta E. \tag{26}$$

In the experiments which have been done on CH_4 to date (18, 28-34) all the vibrational modes have been coupled very rapidly by CH_4-CH_4 collisions (on the order of 70 collisions to couple modes ν_3 and ν_4,[28] and less than 100 collisions to couple modes ν_2 and ν_4).[32] Since this coupling presumably takes place via intermolecular V-V transfer in high concentrations of CH_4, the modes are likely to be much more slowly coupled in dilute mixtures of CH_4. On the basis of his experimental data Yardley concludes[32] that the rate of coupling by rare gases is probably at least a factor of ten slower. Although atmospheric species such as N_2 and O_2 probably behave more like rare gases than like CH_4, we shall nevertheless, assume that all the modes are strongly coupled, since there is not enough data on vibrational relaxation in CH_4 to justify a more detailed description. Furthermore, the symmetric and asymmetric bending modes, ν_2 and ν_4, have comparable vibrational frequencies and are likely to behave similarly, whether coupled or not. The stretching modes, ν_1 and ν_3, have much larger vibrational frequencies and probably relax much more slowly than the bending modes. They will therefore have little effect on the relaxation of CH_4 except to increase the effective degeneracy of the bending levels to which they are coupled. On the basis of these considerations we adopt the model shown in Fig. 5.

The relaxation of CH_4 in the atmosphere is dominated by V-V transfer to O_2 and H_2O. The rate of transfer from CH_4 to O_2 is well documented,[31] although it is not known whether it takes place from near-resonant (0100) level or the infrared active (0001) level. Under the assumption that these levels are in equilibrium with each other we assign this process a room temperature rate equal to 6×10^{-13} cm^3/s in the exothermic direction (O_2 transfer to CH_4). The reverse rate is obtained by detailed balance, using the partition function of the combined CH_4 (0001) and CH_4 (0101) levels. To scale this rate to higher levels we use the harmonic oscillator rule, as before. To scale this rate to different temperatures we assume that the reaction is sufficiently near resonance for the probability per collision to vary as T^{-1}. The rate coefficient in this case varies as $T^{-1/2}$.

The rate of V-V transfer to $H_2O(\nu_2)$ is not so well documented, and there is some controversy regarding the extraction of rate coefficients from the limited data on CH_4/H_2O mixtures.[17, 30] If we accept Bauer's interpretation of the data, the rate of transfer from H_2O (010) to $CH_4(\nu_2 + \nu_4)$ is 6×10^{-11} cm^3/s at room temperature. To scale this rate to higher levels the harmonic oscillator rule is used, as before. To scale the rate to other temperatures we assume that the reaction is sufficiently near resonance that the rate varies as $T^{-1/2}$, as was assumed for transfer to O_2. The subsequent relaxation of $H_2O(\nu_2)$ and O_2 was discussed in Section II-B. 3.

These processes are summarized in Fig. 6, where the relaxation times indicated correspond to the same atmospheric conditions as in Figs. 2 to 5. Only a very small amount of heating or cooling occurs at the absorption of a laser photon by CH_4. At sufficiently low H_2O concentrations ($\ll 0.2\%$) some cooling will occur on the fast time scale ($\sim 4 \times 10^{-6}$s in Fig. 6) corresponding to transfer to O_2. Such small concentrations of H_2O can occur at high altitudes, since H_2O is not uniformly distributed throughout the atmosphere. Although V-V transfer from CH_4 (ν_2 and ν_4) to H_2O (ν_2) is endothermic, this process will not lead to cooling because the H_2O (ν_2) vibration is quenched on the same time scale with a large release of heat. Thus, under conditions of sufficiently high humidity ($\gg 0.2\%$ H_2O), which ordinarily prevail at low altitudes, the laser energy absorbed by CH_4 will lead to heating on a fast time scale ($\sim 7 \times 10^{-7}$s) corresponding to transfer to H_2O (ν_2) and quenching of the H_2O (ν_2) (principally by H_2O itself). The energy transferred to O_2 will appear as heat on a longer time scale ($\sim 10^{-4}$s) corresponding to the relaxation of O_2 via H_2O (ν_2).

6. Kinetics of Absorption of DF Laser Radiation by HDO

HDO absorbs DF laser radiation on the ν_1 fundamental transition

$$HDO\ (000) + h\nu \rightarrow HDO\ (100) + \Delta E. \qquad (27)$$

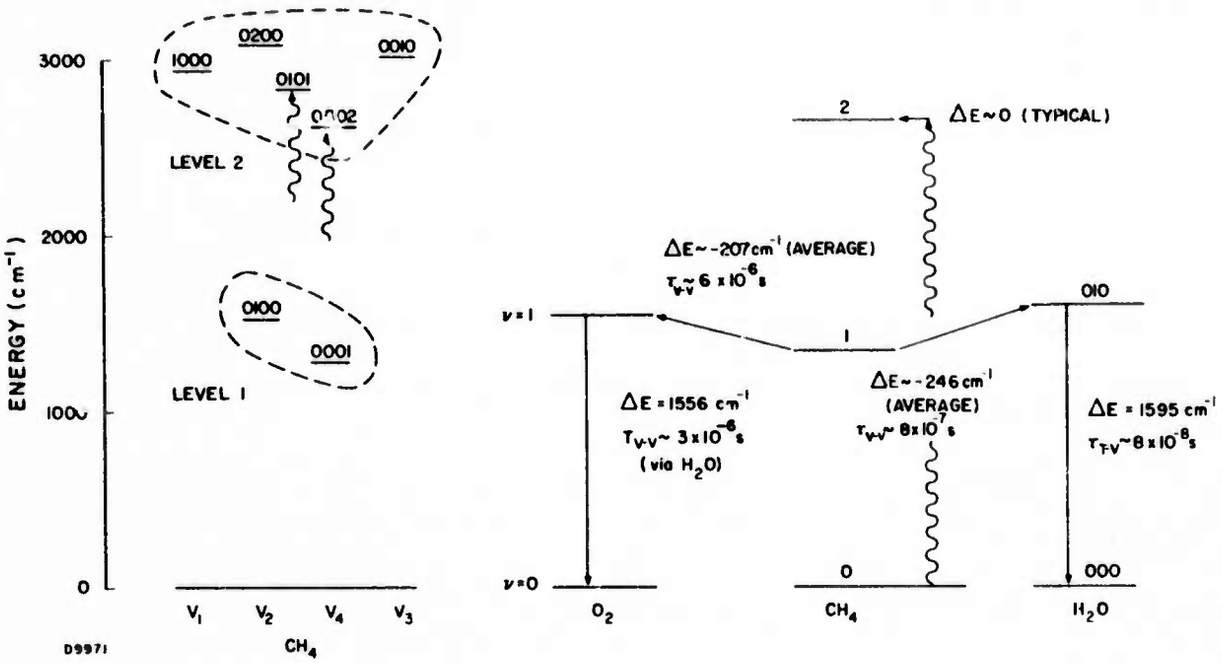

Fig. 6 Kinetics of Absorption of DF Laser Radiation by CH_4

No data exist regarding the relaxation of HDO (ν_1) (or ν_2 or ν_3, for that matter). However, preliminary data have been obtained at AERL regarding the relaxation of H_2O (ν_1) in collisions with H_2O.[35] These data indicate that modes ν_1 and ν_2 (and ν_3 as well) are coupled at every H_2O - H_2O collision, despite the fact that the levels are separated by about 500 cm^{-1}. Because of the similarity of HDO and H_2O, we assume that HDO (ν_1) and (ν_2) are coupled to each other and to H_2O (ν_2) at every collision by the reactions

$$HDC\ (100) + H_2O \rightarrow HDO\ (020) + H_2O \tag{28}$$

$$H_2O\ (010) + HDO\ (000) \rightarrow H_2O\ (000) + HDO\ (010). \tag{29}$$

These reactions are assumed to have rate constants equal to 5×10^{-11} cm^3/sec. To scale to higher levels, the harmonic oscillator rules are used. The T-V relaxation of HDO (ν_2) by H_2O, N_2 and O_2 is assumed to be the same as for H_2O (ν_2).

In addition to these rapid H_2O - HDO processes, near resonant V-V transfer to N_2 and O_2 may be important, especially under conditions of low humidity:

$$O_2\ (v = 1) + HDO\ (000) \rightarrow O_2\ (v = 0) + HDO\ (010) + 153\ cm^{-1}, \tag{30}$$

$$HDO\ (100) + N_2\ (v = 0) \rightarrow HDO\ (000) + N_2\ (v = 1) + 393\ cm^{-1}. \tag{31}$$

The rate of reaction (30) is estimated to be about 1.0×10^{-12} cm^3/s. This is slightly slower (30%) than the corresponding rate of transfer between H_2O (010) and O_2, which is more nearly resonant. It is more difficult to estimate the rate of reaction (31). Due to the larger nonresonance, compared with reaction (30), the rate of reaction (31) has somewhat arbitrarily been assumed to be 2×10^{-13} cm^3/s, which is a factor of five slower than reaction (30).

These processes are summarized in Fig. 7, where the times indicated correspond to the same atmospheric conditions as in Figs. 2 to 6. The dominant effect of absorption by HDO (ν_1) is seen to be rapid heating on a time scale of the order of 4×10^{-8} s, corresponding to the quenching of HDO (ν_2) and H_2O (ν_2) by H_2O.

C. RELAXATION EQUATIONS

With these approximations it is a simple matter to write down the kinetic equations describing the relaxation of the system. For this purpose we shall refer to a group of closely coupled vibrational and rotational states as "level i", and define the partition function Q_i and mean energy ϵ_i for level i by the expressions

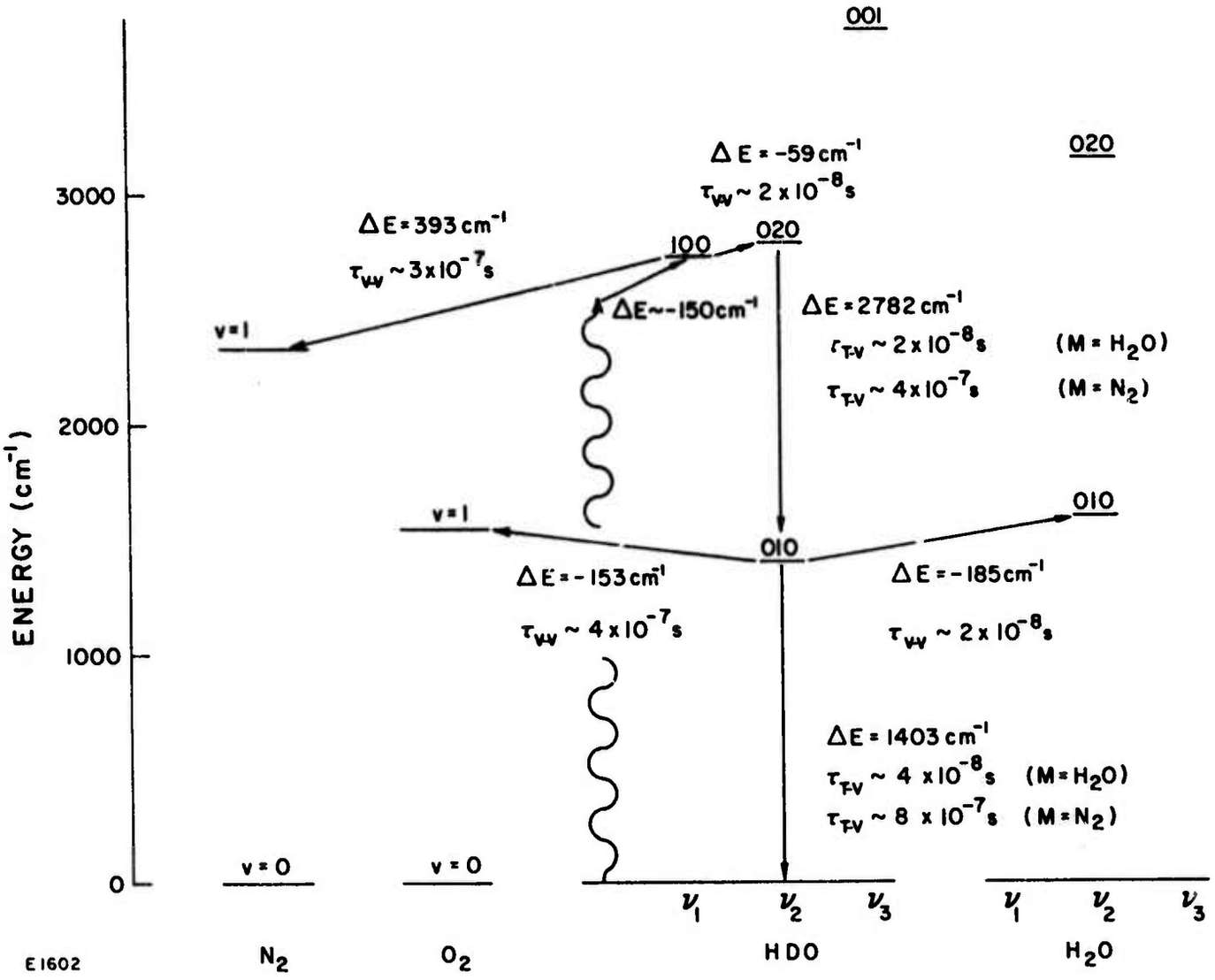

Fig. 7 Kinetics of Absorption of DF Laser Radiation by HDO

$$Q_i = \sum_m g_m \, e^{-E_m/kT}, \tag{32}$$

$$Q_i \epsilon_i = \sum_m g_m \, E_m \, e^{-E_m/kT}, \tag{33}$$

where g_m is the degeneracy of state m, E_m is the energy of state m, k is Boltzmann's constant and T is the temperature.

The density n_i of molecules in level i satisfies the inviscid equation

$$\frac{Dn_i}{Dt} + n_i \nabla \cdot \vec{v} = -\sum_{j,k,\ell} k_{i\to j}^{k\to \ell} \left(n_i n_j - \frac{Q_i Q_k}{Q_i Q_\ell} n_j n_\ell \right) - \sum_{j,\nu} \bar{\sigma}_{i\to j}^{(\nu)} \Phi_\nu \left(n_i - \frac{Q_i}{Q_j} \exp\left(-\frac{h\nu}{kT}\right) n_j \right), \tag{34}$$

where D/Dt is the usual convective derivative, and $\vec{v}$ is the local velocity. Thus, each level of each molecular species is treated as a chemical species capable of undergoing the reactions represented by the right-hand side of the equation. The first term on the right-hand side represents the effect of vibrational relaxation processes of the type

$$A_i + B_k \rightarrow A_j + B_\ell, \tag{35}$$

in which molecule A in level i reacts with molecule B in level k to form molecule A in level j and molecule B in level ℓ, with rate coefficient $k_{i\to j}^{k\to \ell}$. To express this term in the form shown, the usual detailed balance relation

$$k_{i\to j}^{k\to \ell} \, Q_j Q_\ell = k_{j\to i}^{\ell\to k} \, Q_i Q_k \tag{36}$$

has been used. The second term on the right-hand side represents the effect of absorption processes of the type

$$A_i + h\nu \rightarrow A_j \tag{37}$$

and stimulated emission processes of the type

$$A_j + h\nu \quad A_i + 2h\nu. \tag{38}$$

In Eq. (34) $\bar{\sigma}^{(\nu)}_{i\to j}$ is the cross section at the frequency ν and Φ_ν is the flux of photons at this frequency. To express this term in the form shown, the detailed balance relation

$$\bar{\sigma}^{(\nu)}_{i\to j} \quad Q_j = \bar{\sigma}^{(\nu)}_{j\to i} \quad Q_i \exp\ (-\frac{h\nu}{kT}) \tag{39}$$

has been used. This relation is derived in Appendix A.

To solve completely the problem of laser beam propagation it is necessary to solve the vibrational relaxation equations together with the hydrodynamical momentum and energy equations describing the motion of the gas and Maxwell"s equations (or an eiconal approximation) describing the propagation of the beam. However, to simplify the study of absorption kinetics, the effects of beam propagation are ignored, and the laser flux Φ_ν is specified as a function of time. To further streamline the problem, the dydrodynamic effects are approximated by assuming either constant pressure p or constant total density n, where

$$n = \sum_i n_i, \tag{40}$$

$$p = nkT. \tag{41}$$

The constant pressure approximation is appropriate when the laser pulse is so long that a pressure pulse generated by the heating of the gas can propagate beyond the width of the beam. Thus, if W is a characteristic width of the laser beam and Δt is the pulse duration (as seen by a "particle" of gas, in the case of a moving beam) then the constant pressure approximation is valid when

$$a\Delta t/W \gg 1, \tag{42}$$

where a is the speed of sound. For a sound speed a 3×10^4 cm/s, and a beam width W~10cm, we see that the constant pressure approximation is appropriate for pulse lengths $\Delta t > 1$ms. The constant density approximation is appropriate when the laser pulse is so short that a pressure pulse has no time to propagate a significant distance, so that the gas cannot relax hydrodynamically. This limit is valid when

$$a\,\Delta t/W \ll 1. \tag{43}$$

Under the above assumptions, this corresponds to pulse lengths $\Delta t < 100\,\mu s$.

In the constant pressure limit the energy equation may be expressed

$$n\,\frac{D}{Dt}\,\left(\frac{5}{2}\,kT + \bar{\epsilon}\right) = \sum_{\nu,\,i} h\nu\;\Phi_\nu\;n_i\;\sigma_i\,(\nu). \tag{44}$$

where

$$n\bar{\epsilon} = \sum_{i}\;n_i\;\epsilon_i \tag{45}$$

is the total internal (rotational + vibrational) energy. This equation must be solved simultaneously with the relaxation equations. In the constant density limit the energy equation may be expressed

$$n\,\frac{D}{Dt}\,\left(\frac{3}{2}\,kT + \bar{\epsilon}\right) = \sum_{\nu,\,i} h\nu\;I_\nu\;n_i\;\sigma_i\,(\nu). \tag{46}$$

In the remainder of this report, only constant pressure solutions will be discussed. However, the temperature change ΔT is invariably small ($\Delta T/T \ll 1$), so that the relaxation equations are essentially decoupled from the energy equation. Under these conditions the constant density temperature change ΔT_n is simply related to the constant pressure temperature change ΔT_p by the formula

$$\Delta T_n = \frac{5}{3}\;\Delta T_p. \tag{47}$$

III. RESULTS

To completely assess the importance of kinetics for the propagation of DF and CO laser radiation through the atmosphere, it is necessary to survey a wide range of laser parameters (especially intensity and pulse length) and atmospheric conditions (especially altitude and humidity). Although this task has not been completed, preliminary results have been obtained and these are discussed below.

Figures 8 through 15 (interspersed in the text as discussed) give results illustrating the use of our analytical model for atmospheric absorption of DF. Results at CO laser wavelengths are given in Fig. 16. For all cases shown here we have, for simplicity, used a square wave, 30-μs pulse, and assumed the same power level on each laser line with all lasing occurring at the same time. It should be noted that the model is in no way restricted to these conditions.

The concentration of atmospheric absorbers is given in Table V. With the exception of water vapor, which has a variable concentration, the concentrations are determined by the natural atmospheric abundance. For water vapor, we have used two limiting concentrations at sea level which were chosen to represent very dry (2 torr H_2O) and very wet (20 torr H_2O) atmospheres and one representative concentration at 12 km altitude, 5.6×10^{-3} torr H_2O. (All calculations were performed for the sea level temperature of 300°K. The error thus introduced at the higher altitude is probably small. As stated above, absorption by both the N_2 and H_2O continua are neglected.)

Calculations were performed at two altitudes, sea level and 12 km, with 12 km chosen as a reasonable maximum altitude of interest.

TABLE V

CONCENTRATION OF ABSORBING MOLECULES

Absorbing Molecule	Concentration
N_2O	0.28 ppm
CH_4	1.6 ppm
CO_2	330 ppm
H_2O - sea level	20 torr
	2 torr
12 km	5.6×10^{-3} torr
HDO	3×10^{-4} of H_2O concentration

A. ABSORPTION OF DF LASER RADIATION

1. Calculations at Sea Level

Figure 8 presents the translational temperature rise as a function of time during the pulse for each of the atmospheric absorbers separately anf for their sum. (It should be noted that for all the cases we have run, the temperature rise due to a simultaneous absorption by all absorbers is equal to the sum of the individual temperature rises.) The results of this figure represent a reasonable upper bound in that the incident power was taken as 10^7 W/cm^2 on each of the eight laser lines and the water concentration was high (20 torr). (The effect of water concentration on the temperature rise is discussed below and may be obtained by comparing the results of Fig. 8 with those of Fig. 9.) Thermal effects after the power is shut off are not shown in Fig. 8. After the power is shut off, the temperature continues to rise at a reduced rate due to the continuing collisional deactivation of stored vibrational energy. The major absorber under the conditions of Fig. 8 is HDO-H_2O and the effects of CO_2 and CH_4 on the temperature rise are insignificant. Although it is not obvious in the figure, N_2O is slightly bleached under these conditions; i.e., the temperature rise due to N_2O absorption is less than linearly related to the incident power. For the other absorbers, which are not bleached, linear extrapolation to results at lower power levels may be performed.

Figure 9 presents the same information as that shown in Fig. 8 for conditions in which the H_2O concentration is 2 torr, a reasonable lower limit approximating very dry conditions. An obvious difference between Figs. 8 and 9 is that at the lower H_2O concentration in Fig. 9 the total temperature rise is approximately one order of magnitude less than the temperature rise under the 20 torr H_2O conditions of Fig. 8. The effect of the H_2O concentration on the temperature rise is twofold, since H_2O is both a direct absorber of laser energy and a major participant in the kinetics of T-V deactivation.

Because H_2O deactivates both excited N_2O and H_2O-HDO by T-V processes, a higher H_2O concentration results in more absorbed energy appearing as translational energy during the pulse, both for H_2O-HDO and N_2O. Comparing Figs. 8 and 9, it is seen that N_2O has become the major absorber under the conditions of 2 torr H_2O. This is true even though N_2O is more bleached under these conditions than at higher humidity If collisions with water were the only deactivation path available to excited N_2O, then the temperature rise of Fig. 9 due to N_2O would be 0.1 that of Fig. 8. The presence of other deactivation paths makes the difference between the N_2O temperature rise of Figs. 8 and 9 less than a factor of 10. Comparison of the temperature rise due to H_2O-HDO shows the low humidity results to be between 10 and 100 times lower than the high humidity results. Thus N_2O becomes the principal absorber under conditions of low humidity. Here again the effect is due to both lowering the absorber concentration (from 20 to 2 torr) and lowering the deactivator concentration. If collision with water were the only deactivation path

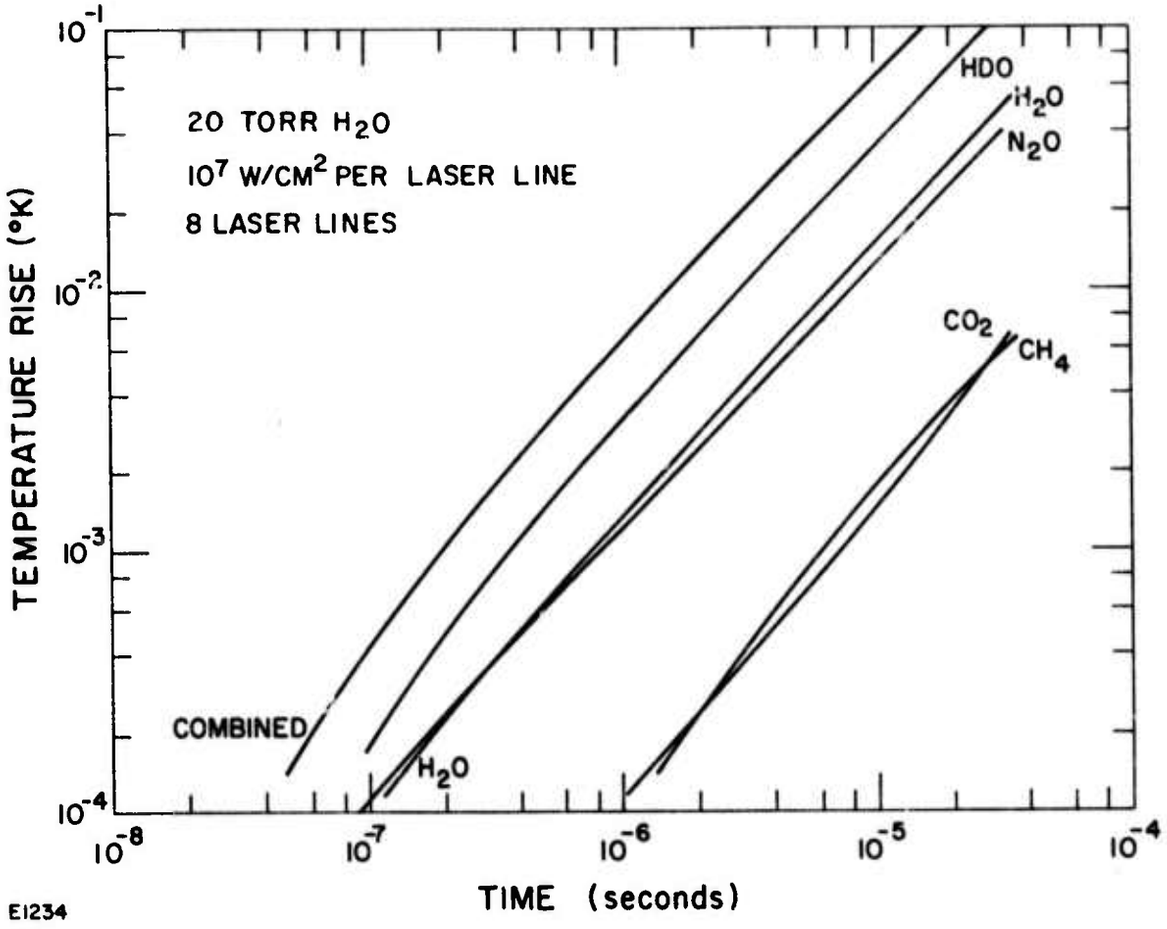

Fig. 8 Translational Temperature Rise for Atmospheric Absorption at DF Laser Wavelengths at Sea Level

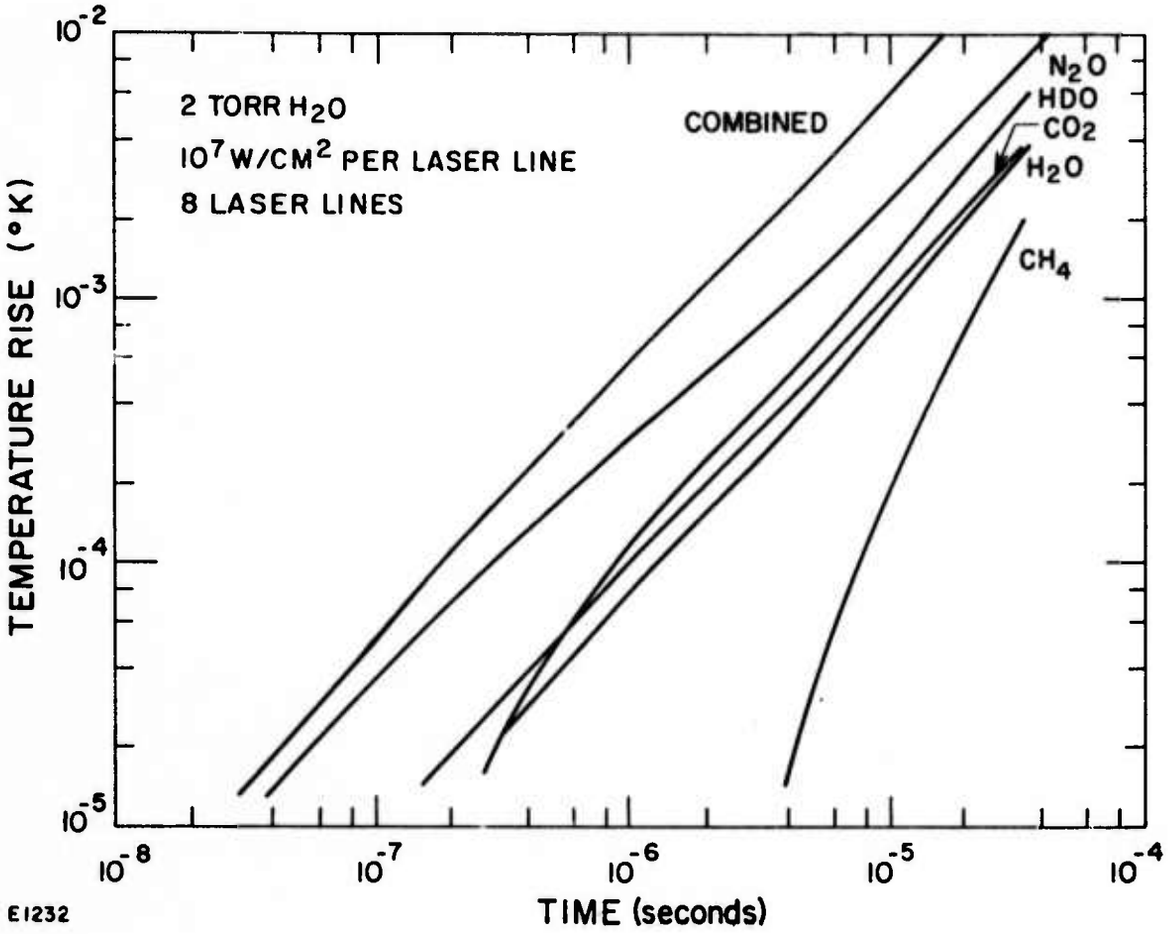

Fig. 9 Translational Temperature Rise for Atmospheric Absorption at DF Laser Wavelengths at Sea Level

available to excited H_2O-HDO, then the H_2O-HDO temperature rise of Fig. 9 would be 0.01 that of Fig. 8. If there were no deactivation path via water, then the temperature rise for H_2O-HDO of Fig. 9 would be 0.1 that of Fig. 8. The fact that there are other deactivation paths available, makes the difference between the H_2O-HDO temperature rise of Figs. 8 and 9 less than a factor of 100 and greater than 10. The differences between the effect of changing the H_2O concentration on absorption by CH_4 and CO_2 are due to the differences between the T-V deactivation effects of H_2O on these two absorbers. These differences are not detailed here because neither is an important absorber.

Figure 10 presents the translational temperature rise as a function of time during the pulse for each of the atmospheric absorbers separately and their sum for an incident power of 10^6 W/cm^2 on each line and a water concentration of 20 torr. (These conditions are the same as those of Fig. 8 except for a factor of 10 lower incident power.) Because N_2O is only very marginally bleached under these conditions, the temperature rise due to N_2O is closer to the total temperature rise than in Fig. 8. Also, the N_2O produced temperature rise may be extrapolated linearly from the results of Fig. 10 to lower power levels. The temperature rise due to all other absorbers is a factor of 10 less than that of Fig. 8.

Figure 11 presents the translational temperature rise at 20 μs due to absorption by N_2O only, as a function of incident power for each of the seven laser lines which are absorbed by N_2O. (Since 3P (8) and 2P (10) have the same cross section for absorption by N_2O, they are presented as one line only resulting in six apparent lines in the figure.) As is expected, the magnitude of the temperature rise is proportional to the N_2O absorption cross section with the largest ΔT for the laser line(s) with the largest N_2O absorption cross section. (These results at 10^7 W/cm^2 are slightly different from those of Fig. 8 because here each line was considered separately. For the case in which all lines are considered together (Fig. 8), the total ΔT is somewhat less than the sum of all lines taken separately since absorption on all lines depletes a common lower state.)

Figure 12 shows, for the laser line of largest N_2O absorption cross section, the power at 20 μs into temperature, transmission, absorption, and stimulated emission, all as a function of incident power for 20-torr H_2O concentration. At all power levels the largest fraction of incident power is transmitted with the absorption in a 1-km path ~ 2% of the transmitted power. When the change in net power absorbed becomes less than linear with increase in incident power, the gas is beginning to become bleached, i.e., the lower state is beginning to become depleted. In Fig. 12 this effect becomes noticeable at an incident power level of ~ 10^6 W/cm^2 on the individual laser line. When the change in net power absorbed (power absorbed minus stimulated emission) with increase in incident power approaches zero, the gas is fully bleached and any further increase in incident power results in no further increase in temperature. Complete bleaching would occur in Fig. 12 at an incident power level significantly higher than those shown here.

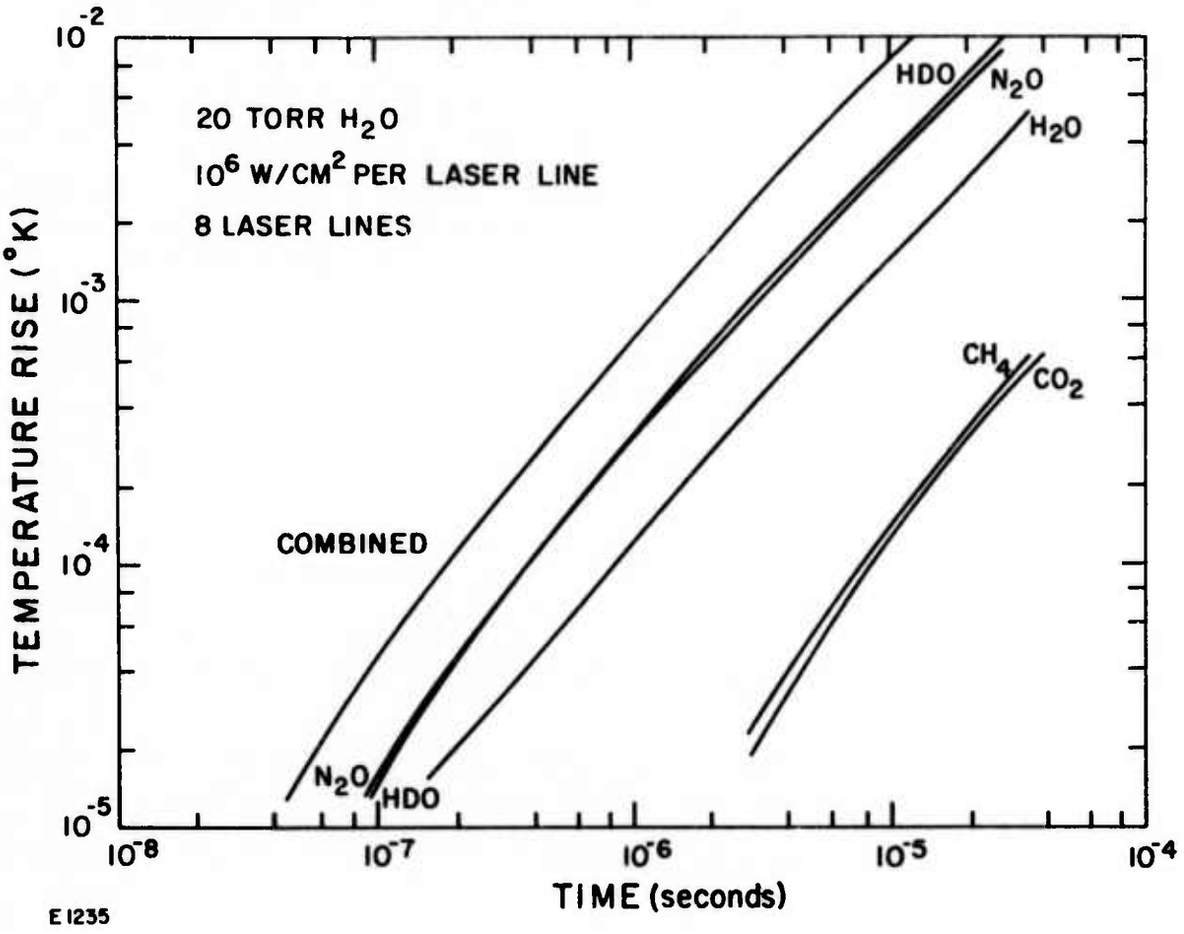

Fig. 10 Translational Temperature Rise for Atmospheric Absorption at DF Laser Wavelengths at Sea Level

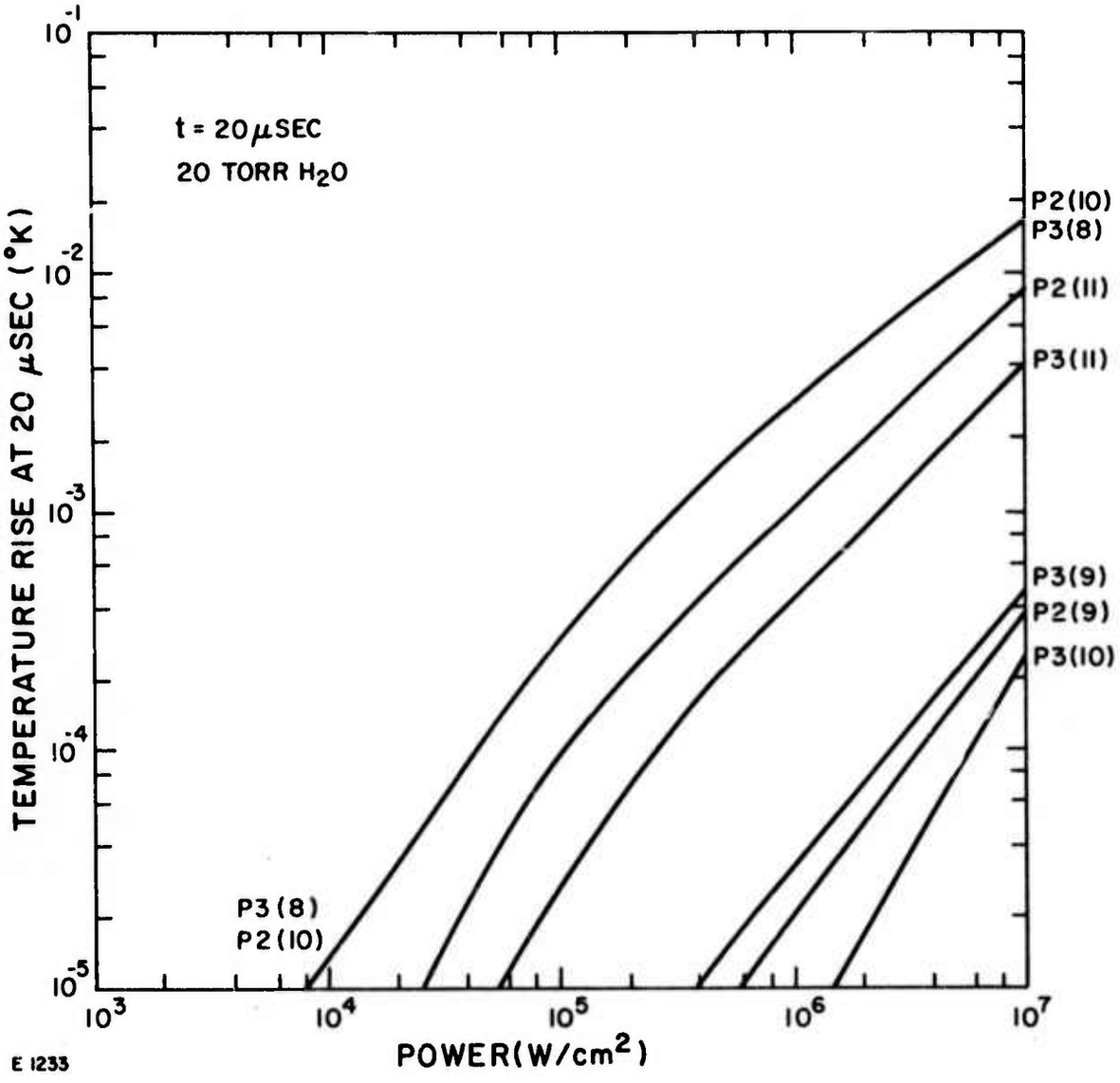

Fig. 11 Translational Temperature Rise for N_2O Absorption at DF Laser Wavelengths as a Function of Incident Power at Sea Level

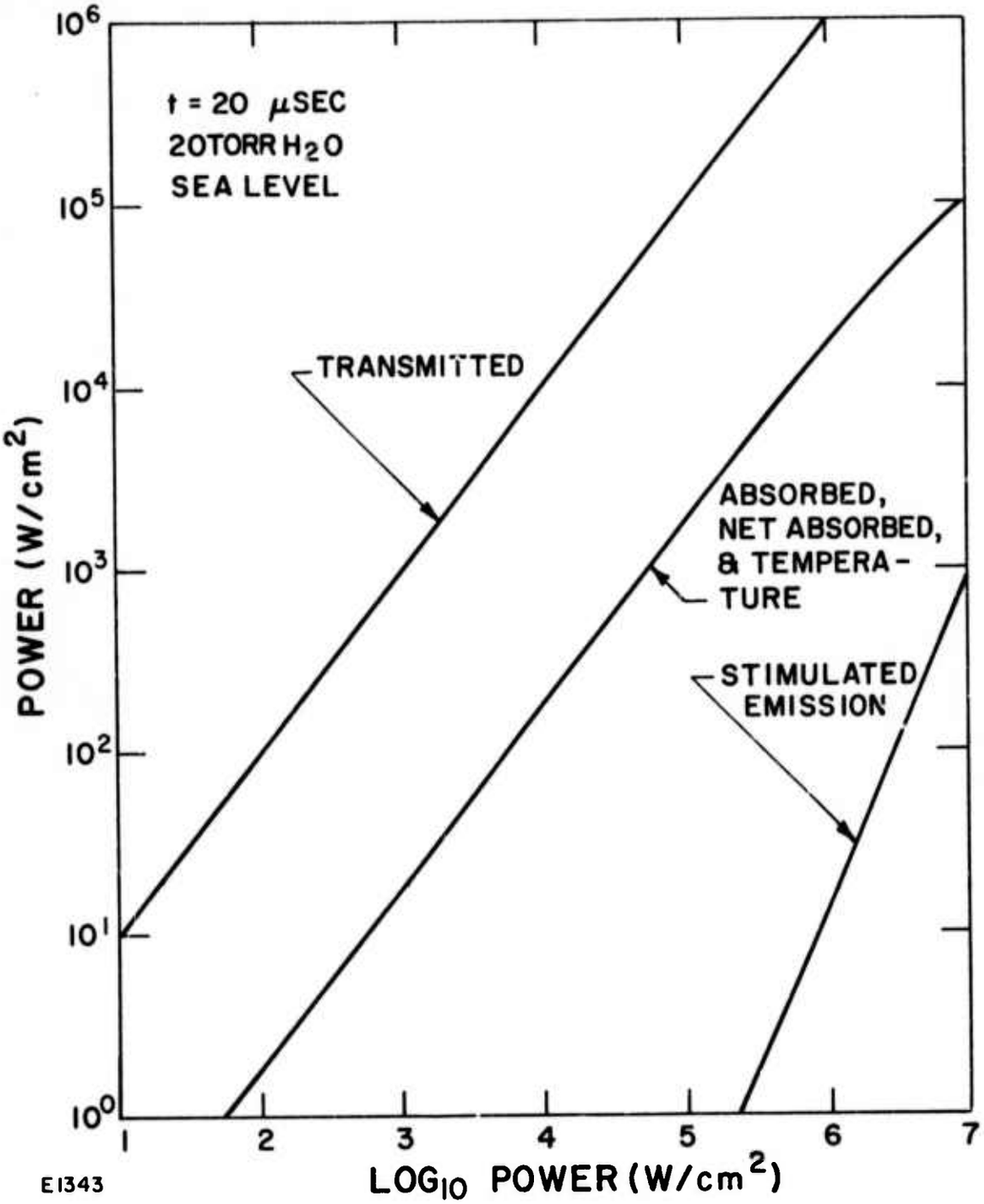

Fig. 12 Power Distribution for Absorption by N_2O of P_2 (10) of Laser Line as a Function of Incident Power

Figure 13 presents the translational temperature rise due to absorption by CH_4 at 220 ppm and 2 ppm under the same conditions as Fig. 8. (The natural concentration of methane in the atmosphere is ~ 2 ppm.) The temperature rise due to DF laser absorption by CH_4, which occurs on only 3 of the 8 laser lines chosen for this study, is linear with CH_4 concentration as expected. If one arbitrarily assumes that the temperature rise due to absorption by some man-made or natural pollutant of interest can be approximated by methane, then the results shown in Fig. 13 indicate that somewhere around a concentration of 100 ppm the pollutant will become the principal absorber of DF laser radiation under the conditions of Fig. 8. Of course, there is no sufficient reason other than convenience to assume absorption and kinetic characteristics for the pollutant similar to those of CH_4, and these results should be treated as of heuristic value only. For any real case of interest, knowledge of the absorption cross section and kinetic scheme would permit the correct calculation to be performed.

2. Calculations at 12 Kilometer Altitude

Figures 14 and 15 present the results of calculations performed at an altitude of 12 km as contrasted to Figs. 8 through 13 which show results for sea level conditions. An altitude of 12 km was chosen to represent a reasonable highest altitude of interest. The water concentration was chosen to be 5.6×10^{-3} torr, which is representative of conditions at 12 km. For calculations at 12 km, the cross sections for absorption were approximately scaled by the decrease in pressure from 1 atm. This is a reasonable procedure because for all the lines of interest, the laser line is far enough away from the absorption line center so that the cross sections scale as the half-width which is linear with pressure for a Lorentz shape line.

Figure 14 presents the 12-km translational temperature rise as a function of time during the pulse for each of the atmospheric absorbers separately and their sum. The incident power was taken as 5×10^6 W/cm^2 on each of the eight lines. Even though N_2O is more bleached than at an incident power level of 10^7 W/cm^2 on each line at sea level (compare slope of ΔT for N_2O here with that of Fig. 8 and also compare Fig. 15 with Fig. 11), N_2O is the principal absorber. Because the H_2O concentration is so low, HDO-H_2O become insignificant contributors to the translational temperature rise. The CO_2 induced temperature rise is almost comparable in magnitude to that of N_2O. The effect of CH_4 absorption under these conditions is to cool the atmosphere causing a temperature decrease. In all cases, the initial slope of ΔT for CH_4 is negative because V-V transfer to O_2 and H_2O is endothermic resulting in net cooling. Under sea level conditions where collisional processes cause rapid equilibration this is a short-lived effect compared to pulse length and net translational heating is rapidly achieved. The reduction in the number of collisions at 12 km results in the cooling effect persisting throughout the time scale of the pulse. As is always true, the eventual result of the absorption of a laser photon is heating, but at 12 km, the time to reach equilibrium is longer than the pulse time for CH_4.

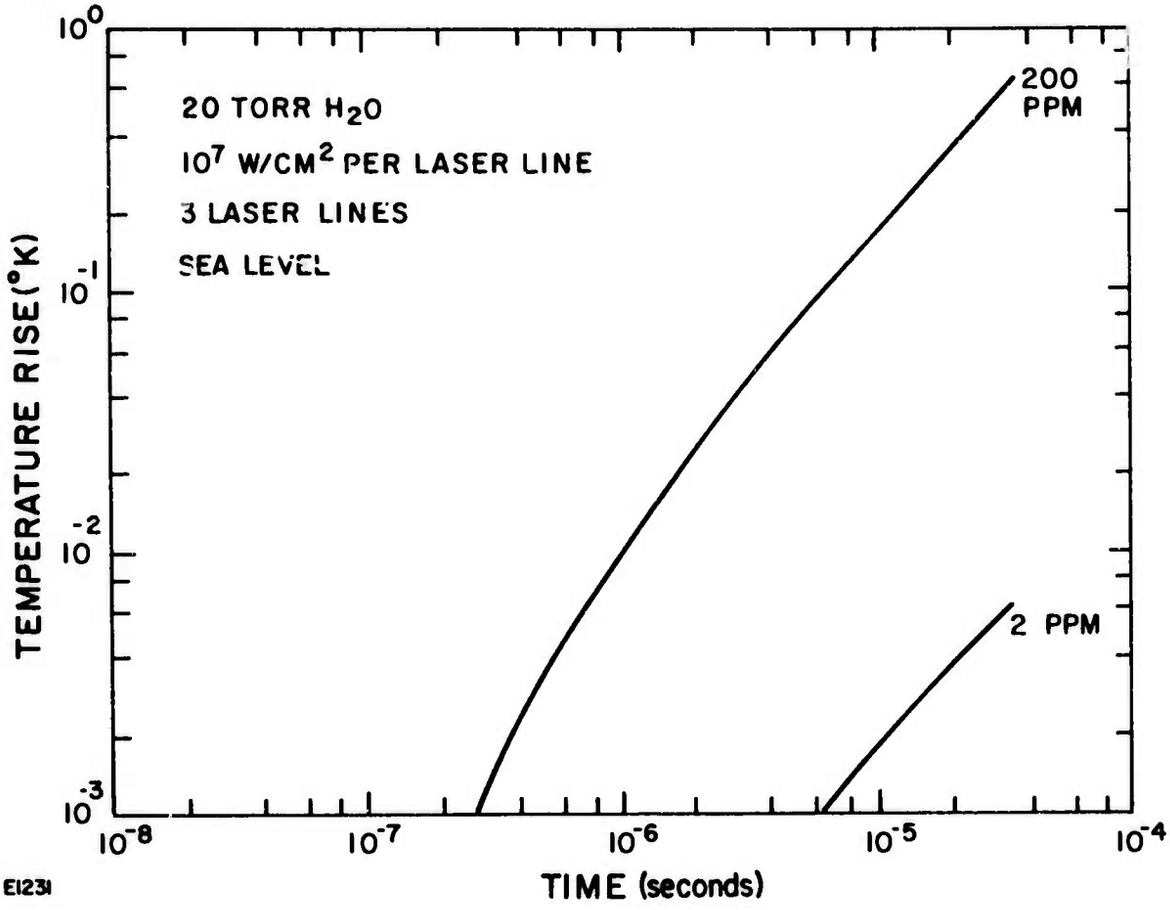

Fig. 13 Translational Temperature Rise Due to Absorption by CH_4 at DF Laser Wavelengths

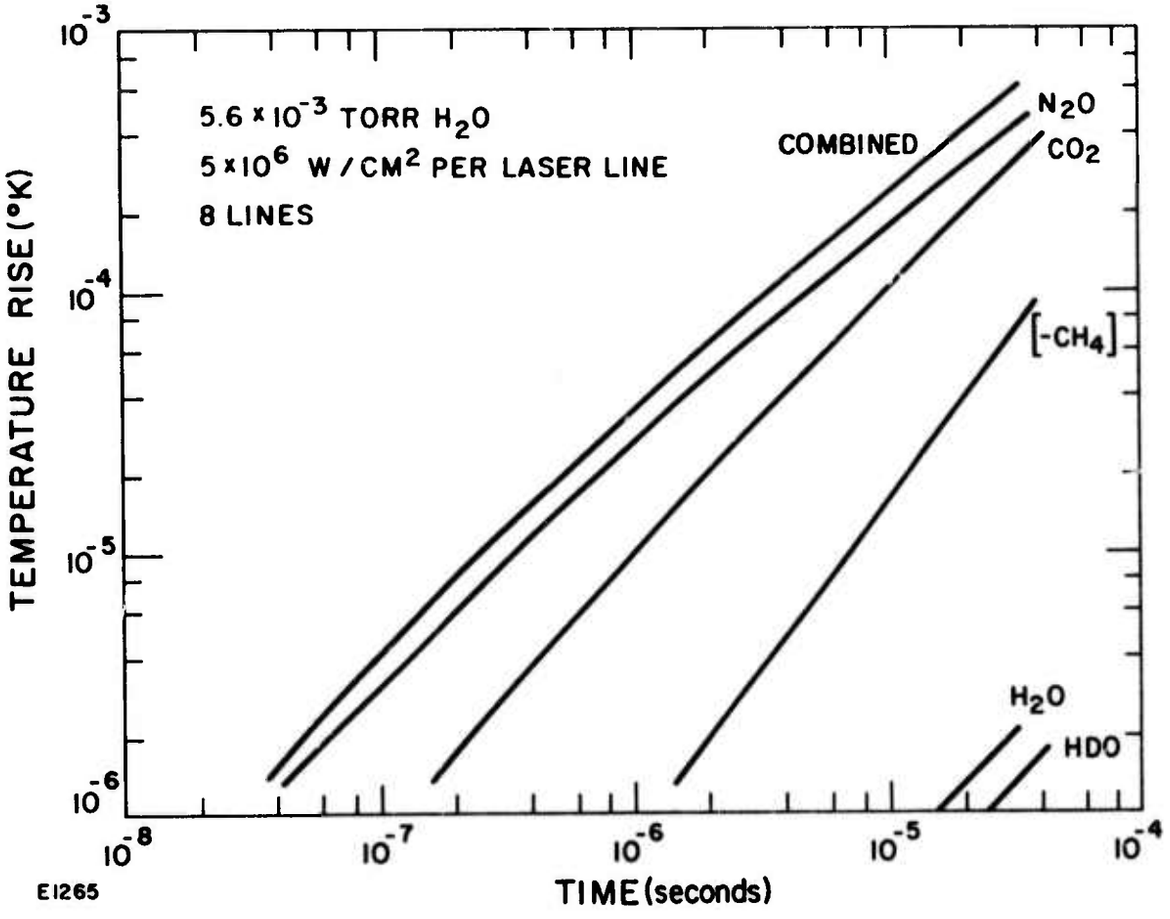

Fig. 14 Translational Temperature Rise for Atmospheric Absorption at DF Laser Wavelengths at 12 km Altitude. (Note CH_4 temperature change is negative)

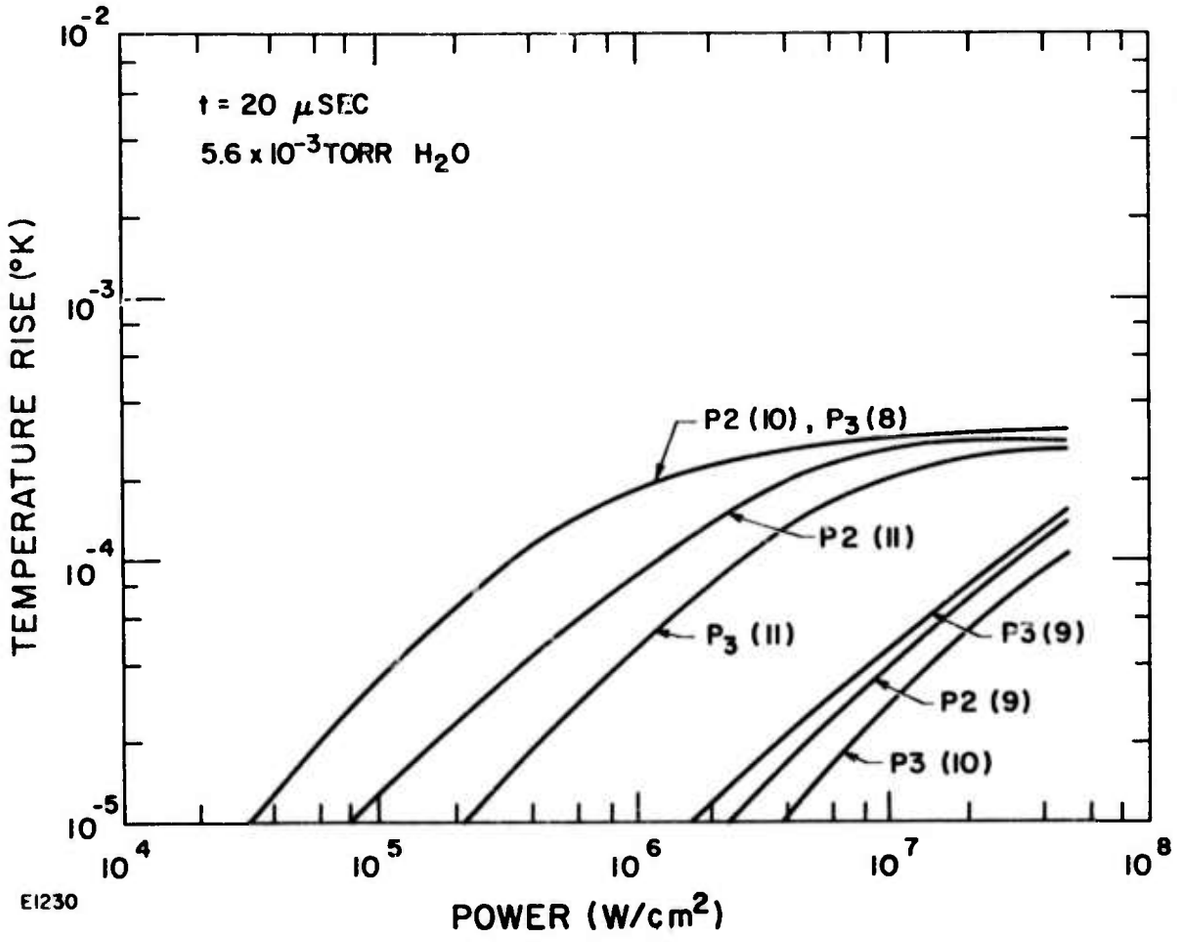

Fig. 15 Translational Temperature Rise for N_2O Absorption at DF Laser Wavelengths as a Function of Incident Power at 12 km Altitude

Figure 15 is the 12-km analog of Fig. 11. It presents the translational temperature rise at 20 μsec due to absorption by N_2O only as a function of incident power. The increased magnitude of bleaching effects at 12 km compared with the sea level conditions of Fig. 11 is easily seen in the steep decrease in slope of ΔT as higher power levels are achieved.

B. ABSORPTION OF CO LASER RADIATION

Figure 16 presents the sea level translational temperature rise as a function of time during the pulse for absorption by H_2O. The results shown here are an upper bound in that the incident power is taken as 10^7 W/cm^2 on each of the 12 CO laser lines given in Table III and the H_2O concentration is 20 torr. Results are presented both for the AERL best estimates of H_2O absorption cross sections and those of McClatchey.[10] The AERL results, as expected from Table III, are almost a factor of three higher. Since there are no bleaching effects, these results can be linearly extrapolated to lower power levels. The important point to be noted here is that the temperature rise due to absorption at CO laser wavelengths is orders of magnitude greater than at DF laser wavelengths for similar conditions.

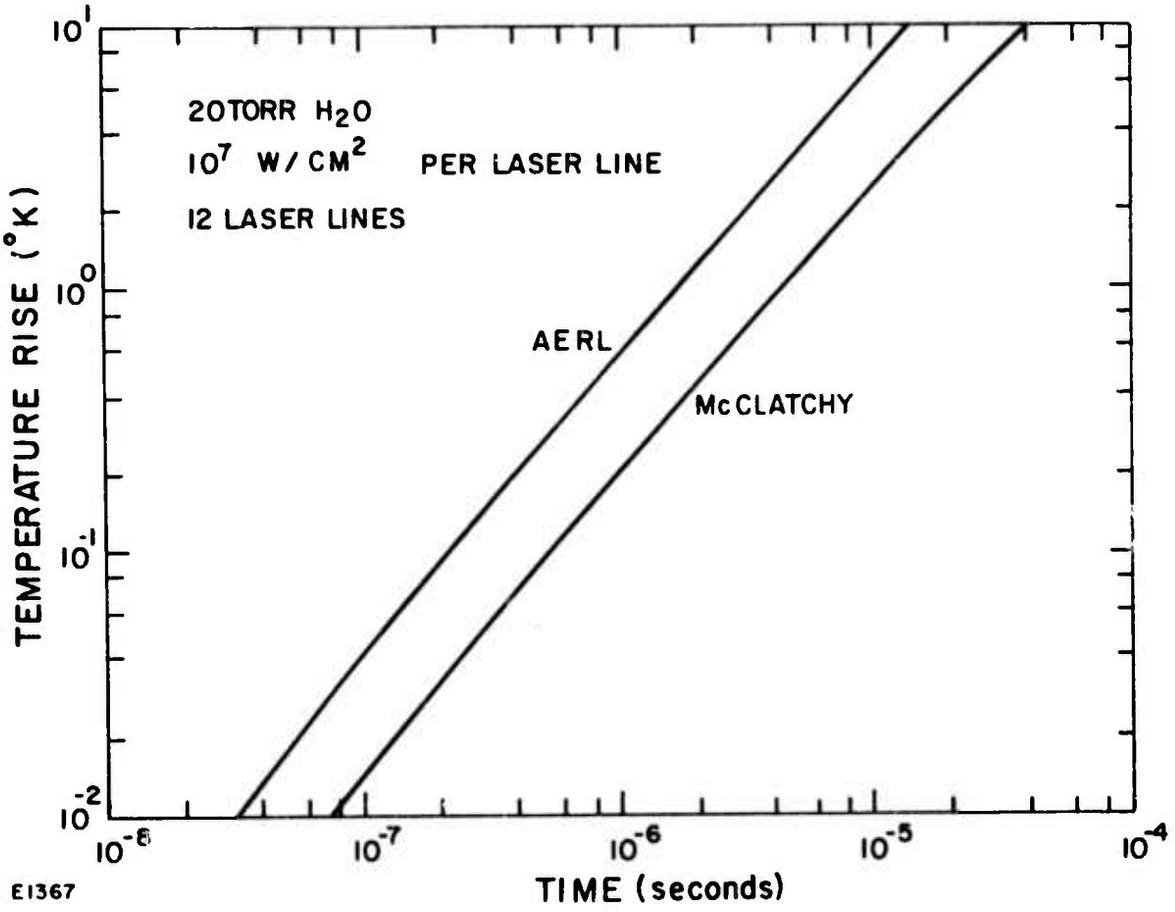

Fig. 16 Translational Temperature Rise for H_2O Absorption at CO Laser Wavelengths at Sea Level

REFERENCES

1. Deutsch, T. F., Appl. Phys. Letters 10, 8, 234 (15 April 1967).

2. Basov, N. G., et al., Appl. Optics 10, 8, 1814 (August 1971).

3. Spencer, D. J., et al., "Atmospheric Gas Absorption at DF Laser Wavelengths," Paper presented at "Absorption of Infrared Laser Radiation in the Atmosphere" Meeting, MITRE Corporation, (April 1973).

4. McClatchey, R. A., et al., AFCRL Atmospheric Absorption Lane Parameters Compilation, Air Force Cambridge Research Laboratories, AFCRL-TR-73-0096, (26 January 1973).

5. Shapiro, M. M., and Gush, H. P., Can. J. Physics 44, 949 (1966).

6. Winters, B. H. et al., "Line Shape in the Wing Beyond the Band Head of the 4.3μ Band of CO_2," J. QSRT 4, 527 (1964).

7. Bates, David M., et al., "Line Parameters and Computer Spectra for Water Vapor Bands at 2.7 Microns," National Bureau of Standards Monograph 71, (3 August 1964).

8a. Mantz, A. W., Nichols, E. R., Alpert, B. D., and Rao, K. N., "CO Laser Spectra Studied with a 10-Meter Vacuum Infrared Grating Spectrograph," J. Mol. Spectry 35, 325 (1970).

8b. Mantz, A. W., Watson, J. K. G., Rao, K. N., Albritton, D. L., Schmeltekopf, A. L., and Zare, R. N., "Rydberg-Klein-Rees Potential for the $X^1\ \Sigma^+$ State of the CO Molecule," J. Mol. Spectry 39, 180 (1971).

9. Long, R. K., Mills, F. S., and Trusty, G. L., "Experimental Absorption Coefficients for Eleven CO Laser Lines," Ohio State University Research Foundation Report No. 3271-5 (March 1973).

10. McClatchey, R. A., AFCRL, private communication

11. McClatchey, R. A., "Atmospheric Attenuation of CO Laser Radiation," AFCRL-71-0370 (1 July 1971).

12. Burch, D. E., France, W. L., and Williams, D., "Total Absorptance of Water Vapor in the Near Infrared," Appl. Opt. 2, 585 (1963).

13. Harris, E. L., and Glowacki, W. J., "Absorption of CO Laser Radiation by Water Vapor Near 5 μm", Naval Ordnance Laboratory Technical Report 73-206 (26 November 1973).

14. Carroll, T. O., and Marcus, S., Physics Letters 27A, 590 (1968).

15. Evans, L. B., "Rotational Relaxation in Polar Gases," Ph. D. Thesis, Oklahoma State University (August 1969).

16. Kley, D., and Welge, K. H., J. Chem. Phys. 49, 2870 (1968).

17. For surveys of vibrational relaxation rates and references to the original papers see: Taylor, R. L., and Bitterman, S., Rev. Mod. Phys. 41, 26, (1969), Moore, C. B., Adv. Chem. Phys. 23, 41, (1973), Lewis, P., et al., "Survey of Vibrational Relaxation Data," Avco Everett Research Laboratory Technical Memorandum (umpublished).

18. Cottrell, T. L., Macfarlane, I. M., Read, A. W., and Young, A. H., Trans. Faraday Soc. 62, 2655 (1966).

19. Cottrell, T. L., Macfarlane, I. M., and Read, A. W., Trans. Faraday Soc. 63, 2093 (1967).

20. Bates, R. D., Flynn, G. W., and Ronn, A. M., J. Chem. Phys. 49, 1432 (1968).

21. Yardley, J. T., J. Chem. Phys. 49, 2816 (1968).

22. Sharma, R. D., J. Chem. Phys. 49, 5195 (1968).

23. Stark, E. E., Appl. Phys. Lett. 23, 335 (1973).

24. Cannemeijer, F., and De Vries, A. E., Physica 70, 135 (1973).

25. The authors are indebted to Moore, C. B., for pointing out this interpretation of Yardley's data.

26. Widom, B., and Bauer, S. H., J. Chem. Phys. 21, 1670 (1953).

27. Sharma, R. D., J. Chem. Phys. 54, 810 (1971).

28. Yardley, J. T., and Moore, C. B., J. Chem. Phys. 45, 1066 (1966).

29. Monkewicz, A. A., J. Acoust. Soc. Am. 42, 258 (1966).

30. Bauer, H. J., J. Acoust. Soc. Am. 44, 285 (1968).

31. Yardley, J. T., and Moore, C. B., J. Chem. Phys. 48, 14 (1968).

32. Yardley, J. T., and Moore, C. B., J. Chem. Phys. 49, 1111 (1968).

33. Evans, L. B., and Winter, T. G., J. Acoust. Soc. Am. 45, 515 (1969).

34. Yardley, J. T., Fertig, M. N., and Moore, C. B., J. Chem. Phys. 52, 1450 (1970).

35. Kung, R. T., (private communication).

APPENDIX A

DETAILED BALANCE FOR OPTICAL TRANSITIONS

We consider a molecule N whose manifold of internal levels may be grouped into two sets of levels, with one set loosely referred to as the ground state, N^o, and the other loosely referred to as the excited state N^*. The total populations of these states are

$$N^o = \sum_i N_i, \tag{A-1a}$$

$$N^* = \sum_j N_j, \tag{A-1b}$$

where N_i and N_j are the populations of the individual levels i and j, respectively. We shall assume that rapid collisional processes keep the relative populations of the levels within each state in equilibrium with each other at the temperature T. That is,

$$N_i = \frac{g_i \exp(-E_i/kT)}{Q^o} N^o, \tag{A-2a}$$

$$N_j = \frac{g_j \exp(-E_j/kT)}{Q^*} N^*, \tag{A-2b}$$

where g_i and g_j are the degeneracies of levels i and j, respectively and E_i and E_j are the energies (referred to the same zero) of levels i and j, respectively, and k is Boltzmann's constant. The partition functions are defined by the expressions

$$Q^o(T) = \sum_i g_i \exp(-E_i/kT), \tag{A-3a}$$

$$Q^*(T) = \sum_j g_j \exp(-E_j/kT). \tag{A-3b}$$

We now suppose that the molecules are subjected to radiation of intensity I_ν and frequency ν, where

$$h\nu = E_j - E_i, \tag{A-4}$$

and h is Planck's constant. The rate of induced transitions is then

$$\dot{N}^* = -\dot{N}^o = N_i B_{ij} I - N_j B_{ji} I, \tag{A-5}$$

where B_{ij} and B_{ji} are Einstein's coefficients for the transitions $i \rightarrow j$ and $j \rightarrow i$, respectively. These coefficients satisfy the relation

$$g_i B_{ij} = g_j B_{ji}. \tag{A-6}$$

Substituting Eqs. (A-2), (A-4) and (A-6) into Eq. (A-5) we obtain the result

$$\dot{N}^* = -\dot{N}^o = \sigma_{\nu i} \Phi_\nu \left[N^o - \frac{Q^o}{Q^*} e^{-h\nu/kT} N^* \right], \tag{A-7}$$

where the flux of photons is

$$\Phi_\nu = I_\nu / h\nu, \tag{A-8}$$

and the absorption cross section for a ground state molecule is defined by the expression

$$\sigma_{\nu i}(T) = \frac{g_i \exp(-E_i/kT}{Q^o} \; h\nu B_{ij}. \tag{A-9}$$

It should be noted that if several transitions are absorbing at the frequency ν, Eq. (A-7) may be used simply by replacing $\sigma_{\nu i}$ by σ_ν, where

$$\sigma_\nu = \sum_i \sigma_{\nu i}. \tag{A-10}$$

If several frequencies ν are being absorbed, separate equations must be written for each frequency.

APPENDIX B

PARTITION FUNCTIONS

1. N_2O "States"

Referred to the elemental chemical species, the partition function (Q) for a molecule in vibrational level $(v_1 v_2 \ell v_3)$ is given by the expression

$$Q_{v_1 v_2 \ell v_3} = \exp(-\Delta H_F^{\circ}/kT) Q^{(T)} Q^{(VR)\ell}_{v_1 v_2 v_3}, \tag{B-1}$$

where ΔH_F° is the heat of formation of $0^{\circ}K$, k is Boltzmann's constant and T is the temperature. The transitional partition function $[Q^{(T)}]$ is given by the expression

$$Q^{(T)} = (2\pi mkT/h^2)^{3/2}, \tag{B-2}$$

where m is the molecular mass and h is Planck's constant. According to the classical rigid rotor approximation, the vibration-rotation partition function $[Q^{(VR)}]$ may be expressed

$$Q^{(VR)\ell}_{v_1 v_2 v_3} = g_\ell \, kT/B_{v_1 v_2 \ell v_3}$$

$$X \exp\left[\left(B_{v_1 v_2 \ell v_3} \ell^2 - G_{v_1 v_2 \ell v_3}\right)/kT\right], \tag{B-3}$$

where $B_{v_1 v_2 \ell v_3}$ is the rotational constant and $G_{v_1 v_2 \ell v_3}$ is the vibrational energy. The vibrational degeneracy is given by the formula

$$g_\ell = 1 \text{ for } \ell = 0,$$

$$= 2 \text{ otherwise.} \tag{B-4}$$

When the vibrational levels are grouped into closely coupled "states", we obtain the following partition functions:

$$Q_0 = Q_{00^0 0} \tag{B-5a}$$

$$Q_1 = Q_{01'0} \tag{B-5b}$$

$$Q_2 = Q_{02^0 0} + Q_{02^2 0} + Q_{100} \tag{B-5c}$$

$$Q_3 = Q_{03'0} + Q_{03^3 0} + Q_{11'0} \tag{B-5d}$$

$$Q_4 = Q_{04^0 0} + Q_{04^2 0} + Q_{04^4 0} + Q_{12^0 0} + Q_{12^2 0} + Q_{20^0 0} \tag{B-5e}$$

2. CH_4 "States"

Referred to the elemental chemical species, the partition function for a molecule in vibrational level $(v_1 v_2 v_3 v_4)$ is given by the expression

$$Q_{v_1 v_2 v_3 v_4} = \exp(-\Delta H_F^{\circ}/kT)\, Q^{(T)} Q^{(VR)}_{v_1 v_2 v_3 v_4} \tag{B-6}$$

where ΔH_F° is the heat of formation of $0^{\circ}K$, k is Boltzmann's constant and T is the temperature. The translational partition function is given by the expression

$$Q^{(T)} = (2\pi\, mkT/h^2)^{3/2} \tag{B-7}$$

where m is the molecular mass and h is Planck's constant. To calculate the vibration-rotation partition function we ignore the fine multiplet splitting of the intercombination levels, and neglect vibration-rotation interaction. The vibration-rotation partition function may then be expressed

$$Q^{(VR)}_{v_1 v_2 v_3 v_4} = \frac{g_v}{12}\left(\frac{kT}{B}\right)^{3/2} \exp\left(-\frac{G_{v_1 v_2 v_3 v_4}}{kT}\right), \tag{B-8}$$

where B = 5.24059 cm^{-1} is the rotational constant and $G_{v_1 v_2 v_3 v_4}$ is the vibrational energy. The vibrational degeneracy is given by the formula

$$g_v = \frac{1}{4} (v_2+1) (v_4+1) (v_4+2) (v_3+1) (v_3+2), \qquad \text{(B-9)}$$

and the factor 12 accounts for the rotational symmetry.

When the vibrational levels are grouped into closely coupled "states", we obtain the following partition functions:

$$Q_0 = Q_{0000} \qquad \text{(B-10a)}$$

$$Q_1 = Q_{0001} + Q_{0100} \qquad \text{(B-10b)}$$

$$Q_2 = Q_{0002} + Q_{0101} + Q_{0200} \qquad \text{(B-10c)}$$

$$+ Q_{1000} + Q_{0010} \qquad \text{(B-10d)}$$

APPENDIX C

SUMMARY OF VIBRATIONAL RELAXATION PROCESSES AND RATES

	Process	Rate k (cm^3/sec)
(1)	$N_2(v=1) + H_2O \rightarrow N_2(v=0) + H_2O$	3.6×10^{-15}
(2)	$N_2(v=1) + N_2 \rightarrow N_2(v=0) + N_2$	2.5×10^{-24}
(3)	$N_2(v=1) + O_2 \rightarrow N_2(v=0) + O_2$	2.5×10^{-24}
(4)	$N_2(v=1) + O_2(v=0) \rightarrow N_2(v=0) + O_2(v=1)$	1.6×10^{-18}
(5)	$CO_2(001) + N_2(v=0) \rightarrow CO_2(000) + N_2(v=1)$	5.4×10^{-13}
(6)	$CO_2(001) + H_2O \rightarrow CO_2(030) + H_2O$	4.3×10^{-13}
(7)	$CO_2(001) + N_2 \rightarrow CO_2(030) + N_2$	1.9×10^{-15}
(8)	$CO_2(001) + O_2 \rightarrow CO_2(030) + O_2$	1.9×10^{-15}
(9)	$CO_2(001) + CO_2 \rightarrow CO_2(030) + CO_2$	4.2×10^{-15}
(10)	$CO_2(001) + H_2O \rightarrow CO_2(000) + H_2O$	4.2×10^{-15}
(11)	$CO_2(030) + CO_2(000) \rightarrow CO_2(020) + CO_2(010)$	1.0×10^{-11}
(12)	$CO_2(020) + CO_2(000) \rightarrow CO_2(010) + CO_2(010)$	6.9×10^{-12}
(13)	$CO_2(100) + \text{anything} \rightarrow CO_2(020) + \text{anything}$	1.0×10^{-10}
(14)	$CO_2(010) + H_2O \rightarrow CO_2(000) + H_2O$	1.8×10^{-11}
(15)	$CO_2(020) + H_2O \rightarrow CO_2(010) + H_2O$	3.6×10^{-11}
(16)	$CO_2(030) + H_2O \rightarrow CO_2(020) + H_2O$	5.4×10^{-11}
(17)	$CO_2(010) + N_2 \rightarrow CO_2(000) + N_2$	3.3×10^{-15}
(18)	$CO_2(020) + N_2 \rightarrow CO_2(010) + N_2$	7.6×10^{-15}
(19)	$CO_2(030) + N_2 \rightarrow CO_2(020) + N_2$	1.1×10^{-14}
(20)	$CO_2(010) + O_2 \rightarrow CO_2(000) + O_2$	3.8×10^{-15}

	Process	Rate k (cm^3/sec)
(21)	$CO_2(020) + O_2 \rightarrow CO_2(010) + O_2$	7.6×10^{-15}
(22)	$CO_2(030) + O_2 \rightarrow CO_2(030) + O_2$	1.1×10^{-14}
(23)	$CO_2(010) + CO_2 \rightarrow CO_2(000) + CO_2$	7.2×10^{-15}
(24)	$CO_2(020) + CO_2 \rightarrow CO_2(010) + CO_2$	1.4×10^{-14}
(25)	$CO_2(030) + CO_2 \rightarrow CO_2(020) + CO_2$	2.2×10^{-14}
(26)	$H_2O(010) + H_2O \rightarrow H_2O\,(000) + H_2O$	4.2×10^{-11}
(27)	$H_2O(020) + H_2O \rightarrow H_2O(010) + H_2O$	8.3×10^{-11}
(28)	$H_2O(010) + N_2 \rightarrow H_2O(000) + N_2$	6.0×10^{-14}
(29)	$H_2O(020) + N_2 \rightarrow H_2O(010) + N_2$	1.2×10^{-13}
(30)	$H_2O(010) + O_2 \rightarrow H_2O(000) + O_2$	2.7×10^{-15}
(31)	$H_2O(020) + O_2 \rightarrow H_2O(010) + O_2$	5.4×10^{-15}
(32)	$H_2O(010) + O_2(v=0) \rightarrow H_2O(000) + O_2(v=1)$	1.5×10^{-12}
(33)	$H_2O(020) + O_2(v=0) \rightarrow H_2O(010) + O_2(v=1)$	3.0×10^{-12}
(34)	$O_2(v=1) + H_2O \rightarrow O_2(v=0) + H_2O$	4.3×10^{-14}
(35)	$O_2(v=1) + N_2 \rightarrow O_2(v=0) + N_2$	3.6×10^{-19}
(36)	$O_2(v=1) + O_2 \rightarrow O_2(v=0) + O_2$	3.6×10^{-19}
(37)	$O_2(v=1) + CO_2(000) \rightarrow O_2(v=0) + CO_2(010)$	6.6×10^{-15}
(38)	$N_2O(010) + H_2O \rightarrow N_2O(000) + H_2O$	2.0×10^{-11}
(39)	$N_2O(020) + H_2O \rightarrow N_2O(010) + H_2O$	4.0×10^{-11}
(40)	$N_2O(030) + H_2O \rightarrow N_2O(020) + H_2O$	6.0×10^{-11}
(41)	$N_2O(040) + H_2O \rightarrow N_2O(030) + H_2O$	8.0×10^{-11}
(42)	$N_2O(010) + N_2 \rightarrow N_2O(000) + N_2$	1.8×10^{-14}
(43)	$N_2O(020) + N_2 \rightarrow N_2O(010) + N_2$	3.6×10^{-14}
(44)	$N_2O(030) + N_2 \rightarrow N_2O(020) + N_2$	5.3×10^{-14}

	Process	Rate k (cm^3/sec)
(45)	$N_2O(040) + N_2 \rightarrow N_2O(030) + N_2$	7.1×10^{-14}
(46)	$N_2O(010) + O_2 \rightarrow N_2O(000) + O_2$	1.8×10^{-14}
(47)	$N_2O(020) + O_2 \rightarrow N_2O(010) + O_2$	3.6×10^{-14}
(48)	$N_2O(030) + O_2 \rightarrow N_2O(020) + O_2$	5.3×10^{-14}
(49)	$N_2O(040) + O_2 \rightarrow N_2O(030) + O_2$	7.1×10^{-14}
(50)	$H_2O(010) + N_2O(000) \rightarrow H_2O(000) + N_2O(020)$	1.0×10^{-12}
(51)	$H_2O(010) + N_2O(010) \rightarrow H_2O(000) + N_2O(030)$	1.0×10^{-12}
(52)	$H_2O(010) + N_2O(020) \rightarrow H_2O(000) + N_2O(040)$	2.0×10^{-12}
(53)	$O_2(v=1) + CH_4(0000) \rightarrow O_2(v=0) + CH_4(0001)$	6.0×10^{-13}
(54)	$O_2(v=1) + CH_4(0001) \rightarrow O_2(v=0) + CH_4(0002)$	1.2×10^{-12}
(55)	$H_2O(010) + CH_4(0000) \rightarrow H_2O(000) + CH_4(0001)$	6.4×10^{-11}
(56)	$H_2O(010) + CH_4(0001) \rightarrow H_2O(000) + CH_4(0002)$	1.3×10^{-10}
(57)	$HDO(100) + H_2O \rightarrow HDO(020) + H_2O$	2.0×10^{-10}
(58)	$HDO(000) + H_2O(010) \rightarrow HDO(010) + H_2O(000)$	2.0×10^{-10}
(59)	$HDO(010) + H_2O(010) \rightarrow HDO(020) + H_2O(000)$	4.0×10^{-10}
(60)	$HDO(000) + H_2O(020) \rightarrow HDO(010) + H_2O(010)$	4.0×10^{-10}
(61)	$HDO(010) + H_2O \rightarrow HDO(000) + H_2O$	4.2×10^{-11}
(62)	$HDO(020) + H_2O \rightarrow HDO(010) + H_2O$	8.3×10^{-11}
(63)	$HDO(010) + N_2 \rightarrow HDO(000) + N_2$	6.0×10^{-14}
(64)	$HDO(020) + N_2 \rightarrow HDO(010) + N_2$	1.2×10^{-13}
(65)	$HDO(010) + O_2 \rightarrow HDO(000) + O_2$	2.7×10^{-15}
(66)	$HDO(020) + O_2 \rightarrow HDO(010) + O_2$	5.4×10^{-15}
(67)	$HDO(100) + N_2(v=0) \rightarrow HDO(000) + N_2(v=1)$	2.0×10^{-13}
(68)	$O_2(v=1) + HDO(000) \rightarrow O_2(v=0) + HDO(010)$	1.0×10^{-12}
(69)	$O_2(v=1) + HDO(010) \rightarrow O_2(v=0) + HDO(020)$	2.0×10^{-12}